

Composite polaron formed on surface of two-dimensional lattice system in weak coupling regime

Chen-Huan Wu  *

College of Physics and Electronic Engineering, Northwest Normal University, Lanzhou 730070, China

August 22, 2023

We investigate the properties of composite polaron containing the effects of electron-phonon coupling and interaction between impurity and electron-hole pair. A model of a two-dimensional electron gas occupying the surface of two-dimensional Dirac honeycomb lattice is constructed. We focus on the weak coupling regime throughout the paper. Our results are meaningful to the study of pairing mechanism as well as the phonon-mediated high-temperature superconductivity.

1 Introduction

The mobile impurity is widely studied in ultracold atomic systems like the Fermi gases[1, 82] or Bose-Einstein condensates[2], degenerate Bose-Fermi mixtures[3, 9], and the solid state systems, like the semiconductor[4], (semi) Dirac systems[6, 5] metals[103, 98], and the transition metal dichalcogenides[97]. For both the Mott insulator state[11] and superfluid state[113, 8, 9, 10], the mobile spin impurity as well as the formed polaron (by dressing the particle-hole pairs) are also discussed. In dealing with the many-body problem of the polaron system, the leading order $1/N$ expansion based on the random-phase approximation (RPA) is similar to the self-consistent medium T -matrix which with a dynamically screened interaction (the GW approximation), and the $1/N$ order requires a self-energy term contributed by the particle-hole loop, to describes the pairing fluctuation especially in strong coupling regime like the unitary Fermi gas. At $N \rightarrow \infty$ limit, the self-energy vanishes and the lifetime of the Fermi quasiparticle $\rightarrow \infty$ according to $\text{Re}\Sigma(\text{Im}\Sigma) \sim \frac{1}{N}$ and $\text{Im}\Sigma(\omega) = -\frac{1}{2\tau} \text{sgn}[\omega]$. Here the self-energy is the Coulomb-interaction-induced which including the exchange part and the correlation part, the correlation part here is due to the quantum fluctuations of the Fermi sea, and it leads to the dielectric response. The particle-hole pairs (coupled by the Coulomb potential) as the low-energy excitations are promoted in two-dimensional system[12], In the presence of RPA with the collective electronic modes, the quasiparticles interact with the particle-hole excitations which forms the polaron when the quasiparticle is a mobile impurity, such a scenario can be realized by using a two-dimensional electron gas coupled with the two-dimensional Dirac system or the surface state of three-dimensional Dirac system, the Dirac material here can also be replaced by the topological crystals like the Chern insulator, then the impurity also exhibit some topological features due to the coupling with the environment which is in a topologically nontrivial state[113, 14]. Such scenario can be realized even in the absence of gases but just relies on the exciton-electron interaction within a microcavity diagram [4, 13]. As we known, the plasmon excitation $\omega_p \sim \sqrt{q}$ in long-wavelength limit where q is the scattering momentum, and it obtains more spectral weight when enters into the particle-hole continuum region, due to the Landau damping which leads to a weaker interaction (and thus with larger residue \mathcal{Z} [5]). The coupling between the plasmon and the polaron would be more strong in the massless two-dimensional Dirac system compared to the massive one[15, 16]. The appearing of avoided crossing in the polaron band structure as a result of the strong coupling is also an interesting phenomenon. Furthermore, in the presence of strong coupling, the avoided crossing will disappears gradually with the increase of temperature (away from the superfluid phase again), and then the particle branch merges with the hole branch to form a new (adiabatic) polaron dispersion[82], and this new dispersion is shifted by the binding energy ($-E_b$) or the polaron shift in atomic limit ($t \rightarrow 0$) which is ($-\frac{g^2}{2m_{e-h}\omega_{e-h}^2}$). Besides, in this limit, the polaron conductivity behaves as $\sigma \sim \frac{W}{T} e^{\Omega/T}$ due to the smallness of bandwidth W .

The adiabaticity and non-adiabaticity are closely related to the physical properties of the quantum system[112], including the instability and the phase transitions. In this paper, we consider the composite polaron which is a fermi polaron dressed by the surrounding acoustic phonons, in the surface of a two-dimensional (2D) honeycomb lattice. Unlike the optical phonon modes, the acoustic phonons have a lower energy (which vanishes in the BZ center) and thus provide an effective scattering channel[123]. Also, the energy transition into the acoustic phonon bath is the dominant cooling

*chenhuanwu1@gmail.com

way for the moving electron (impurity)[124]. This energy transition is related to the acoustic phonon dispersion (mainly the linear one). While the effect of surface optical phonons can be exploited by deposit the material on a polar substrate. In adiabatic limit, where the Fermi velocity of electron is much larger than the sound velocity, the electron-phonon scattering is elastic (this is valid even for the neutral limit) and interband transitions vanish, thus the electron will not loss energy. But for another case, when the non-relativistic electron moves faster than the sound wave but still interacts with the acoustic phonons, i.e., in the nonadiabatic regime, the electron may losses energy by the Cherenkov radiabation.

The existence of Dirac cone in 2D lattice can be seen as a perturbation to the free electron (impurity) as discussed in this paper. The resulting mobile polaron exhibits composite dispersion modified by the interaction between impurity and the electron-hole pair as well as the electron-phonon coupling. We find the modification of dispersion induced by weak electron-phonon coupling is linear with the impurity momentum in the stable (adiabatic) regime. While for strong electron-phonon coupling, the avoided crossing appears in the polaron band structure as a result of nonadiabaticity. We know that the band gap in the middle point of Brillouin zone edge will be reduced gradually with the rise of doping level. At the nonadiabatic regime, the band gap in M -point can even disappears, which means that, the excitation (acoustic plasmon mode[98, 102, 107]) can enters into the adjacent Brillouin zone and be free from the influence of umklapp scattering even at higher temperature. The lattice periodicity as well as the Brillouin zone symmetry is missing. In this case, the superfluid can be observed by the crossing Bloch bands at low enough temperature, which can not be stoped by the periodic perturbing potential originates from the lattice[98, 46]. Note that the avoided crossing can also appears in the ultracold fermi atomic systems in strong-interacting limit[82]. The finite temperature effect on the self-energy induced by electron-phonon coupling is also been discussed. In this paper, we set a small fermi energy throughout this paper to avoid the problem of Pauli blocking and support the contact interaction. Also, in nonadiabatic case without the perturbations, we treat the impurity dispersion (kinetic energy) as the conventional non-relativistic electron dispersion which is parabolic.

For the impurity motion-dependent phenomenons, like the coherence or decoherence, which in some degrees related to the Fermi liquid or non-Fermi liquid behavior[119], are important in studying the formation of the polaron. The decoherence process may happen in the extreme case which with a very light impurity immersed into a bath of heavy particles. While in the opposite limit: for a heavy impurity in 1D system, the decoherence can also happen at zero temperature limit due to the orthogonality catastrophe[116, 117, 118]. In adiabatic case, the existence of the absorption and emission of phonons also leads to decoherence effect and reduces the coherent band motion.

To extracting more information about the single and multi-particle excitations and quasiparticles, we apply the method of range-separated hybrid functionals (RSH), where the spacial effect can be estimated in terms of the RSH parameters (for short range and long-range exchange), and a range-separation parameter. Distinct from the generalized gradient approximation (GGA), the method of RSH exhibits better the role of spatial effects, e.g., when the polaron-molecule (dimer ground state) transition happen and for example when a molecule is being stretched or is subject to an applied electric field where charge transfer takes place.

For electron-phonon coupling considered in this paper, we assume the acoustic phonons with large enough sound velocity to ensure the phonon energy ($\hbar\Omega_{ph}$) larger than the band gap, and thus single-phonon linewidth (quantum) is nonzero due to the existence of electron-phonon coupling. For in-plane acoustic phonons near Brillouin zone center, they can cause the intraband carrier transition by the deformation potential scattering, by cannot cause interband carrier transition due to the nonconservation of energy[131, 38, 132]. However, for large enough sound velocity and away from the zone center, the interband transition rate is finite[123] and with a finite scattering angle in the relaxation time approximation. This scattering angle in ladder diagrams will introduces a $(1 - \cos\theta)$ term and related to the chiral characters, which we will discuss indetailin other place[6]. To deal with the impurity-phonon interaction, we apply the Fourier transformed Su-Schrieffer-Heeger (SSH) model[66, 72, 133] where we only consider the carriers transition from valence band to conduction band, and thus the electron-hole recombination does not exists. While in the presence of strong field or the polar substrate, an electric field may be produced by the phonons with high energy, and then the polaronic effect may also comes from the coupling between the electron-hole pair with the ions, as recently realized in ionic solid LiF[134] where the method of optimally tuned and range-separated hybrid functionals (OT-RSH) performs well[120]. Away from the dilute electron density limit[135, 136], in a system that dominated by the coupling strength, a polaron-molecule transition can be realized at a large binding energy, which corresponds to small momentum cutoff during the calculation of two-body coupling function. As an example, in N-type doped transition metal oxides, the localized electrons form the electron-trapped surface polarons can modify the charge transfer and strengthen the polarization. Such charge transfer can weaken or break the covalent bond through the formation of active sites, like the reduced metal ion or the synergistic effect between electron-deficient and electron-rich sites[137]. During this process, the electron transition cleave the existing covalent bond and dissociate the molecule. Such actived covalent bond in the molecules can be experimentally observed through the far-infrared near-field spectrum[139], where the vibrational polaronic dynamics can be directly measured. This can also be realized by applying high pressure to molecular solid can change it into extended structures during which process the repulsive interatomic interactions are weakened[138] and the long-range order will be replaced by the short-range one. In this case, the suppression of long-range order can be estimated by analyzing the deviation between the real charge density distribution with that calculated under range-separated potential. Such phenomenon can be observed in severral materials containing the transition metals, like the amorphous WTe₂ in semiconducting phase[141] and the TiO₂[137, 140], where the hot(thermally-activated) carriers hopping as well as the electron-phonon coupling contribute to the formation of polaron.

2 T -matrix approach and the related coupling between non-relativistic particles

Different to the usual case of a Bose-Fermi mixture in ultracold atomic system, we can assume a two-dimensional weakly-interacting Bose gas coupled to the (two-dimensional) crystal, for average-distance between bosons in the order of van der Waals length l_{vdW} which is comparable or even larger than the s -wave scattering length[19], that's in contrast to the case near Feshbach resonances (with large a) where the weakly-bound three-body states (trimer) would be formed[17, 18]. The van der Waals interaction here can be controlled by choosing materials with different orbital characters. To obtain the analytical solution of the scattering problem, the Bethe-Salpeter equation (BSE) is often reduced to the Lippmann-Schwinger equation (LSE) by ignoring the center-of-mass momenta, i.e., the vacuum T -matrix. The zero center-of-mass momentum can be realized experimentally by increasing the strength of spin-orbit coupling, like the molecule state in BEC limit, note that while for polaron state, the impurity with zero momentum does not correspond to the zero center-of-mass case, the impurity and hole with momentum k_F and $-k_F$, respectively, corresponds to it[52]. The BSE is more difficult to solve due to its singularity[26, 27, 28] especially in the presence of coupled center-of-mass and relative motions by the Fermi sea, it can be described by the non-self-consistent many-body T -matrix[6, 5]

$$\begin{aligned} T(p+q, \square; p+q-k'; \omega) &= g^b(p+q, \square; p+q-k') \\ &= \sum_{k, \Omega} g^b(p+q, \square; k) (-G_0^\phi(p+q-k; \omega+\Omega) G_0^\psi(\square+k; \Omega)) T(p+q-k, \square+k; p+q-k-k'; \omega) \\ &= g^b(p+q, \square; p+q-k') + g^b(p+q, \square; k) \Pi(p+q; \omega) T(p+q-k, \square+k; p+q-k-k'; \omega), \end{aligned} \quad (1)$$

where g^b are the bare impurity-majority interactions, specially, $g^b(p+q, \square; k)$ is the interaction induced by the polarization operator (consist of the two bare Green's functions). k, k' are the relative momentum. G_0^ψ and G_0^ϕ are the bare Fermionic and Bosonic Green's function, as given by $G_0^\psi(\nu, k) = [\nu + i0^+ - \frac{\hbar^2 k^2}{2m_\psi} + \mu_\uparrow]^{-1}$ and $G_0^\phi(\omega + \Omega - \nu, p+q-k) = [\omega + \Omega - i\nu + 2i0^+ - \frac{\hbar^2(p+q-k)^2}{2m_\phi} + \mu_\downarrow]^{-1}$, respectively. $\Pi(p+q)$ is the polarization operator.

By ignoring the harmonic oscillation quantum numbers, and solve the LSE up to first order, we can obtain

$$T(\omega) = \frac{g(\omega)}{1 - g(\omega)\Pi(\omega)}, \quad (2)$$

and thus

$$T^{-1}(\omega) = (g(\omega))^{-1} - \Pi(\omega). \quad (3)$$

Straightly, when we solve the LSE up to second order (we omit the common parameter ω in the following), we have

$$T^{-1} = (g + g^2\Pi)^{-1} - \left(\frac{1}{g\Pi^2} + \frac{1}{\Pi}\right)^{-1}. \quad (4)$$

This T -matrix here is certainly the single channel one due to the infinitely large hyperfine splitting energy, while for finite range case, i.e., both the intraspecies and interspecies (hyperfine levels) coupling are considered, the multichannel T -matrix (consider the center-of-mass frame) becomes[22, 23]

$$T_{12} = \frac{g_1}{1 - g_1\Pi_1} + \left(\frac{g_{12}}{1 - g_1\Pi_1}\right)^2 \frac{1}{\Pi_2^{-1} - g_2 - \frac{(g_{12})^2\Pi_1}{1 - g_1\Pi_1}}, \quad (5)$$

where the subscript 1 denotes the open channel and 2 denotes the close channel.

At first, we discuss the zero energy scattering matrix in the atomic limit in perturbation theory (without consider the effect of hopping). By solving the LSE for low-energy scattering, the regularized intraspecies and bare interspecies coupling parameter (or called the binary contact interaction) can also be obtained[19, 6]

$$\begin{aligned} g_{\phi\phi} &= \frac{4\pi\hbar^2 a_{\psi\psi}}{m_\phi} = \left[\frac{1}{g_{\phi\phi}^b} + \int \frac{d^2k}{(2\pi)^2} \frac{g(k)}{\hbar^2 k^2}\right]^{-1}, \\ g_{\psi\phi}^b(\Lambda) &= \left[\frac{m_r}{2\pi\hbar^2 a} + \int \frac{d^2k}{(2\pi)^2} \frac{1}{\varepsilon_{k\uparrow} + \varepsilon_{k\downarrow}}\right]^{-1}, \\ &= \left[\frac{m_r}{2\pi\hbar^2 a} + \int \frac{d^2k}{(2\pi)^2} \frac{2m_r}{\hbar^2 k^2}\right]^{-1}, \end{aligned} \quad (6)$$

where ϕ denotes the bosonic field, $g_{\phi\phi}^b$ is the bare coupling parameter, here $g_{\phi\phi} < 0$ for attractive interaction. $g(k)$ is the interaction range-dependent function, when it's momentum-independent (for contact interaction or the short-range limit), the integral within the above equation does not converges, then the momentum cutoff is required which is of the order of inversed interaction range, e.g., $\Lambda \sim 1/l_{vdW}$. The cutoff Λ goes to infinite when $g_{\psi\phi}^b$ goes to zero and in this case the average potential energy is zero. This usually corresponds to the short-range limit with very large hyperfine splitting energy between the two lowest energy hyperfine states[23, 25] in open channel and closed channel respectively

for a statistically mixed atomic system (like the fermi-fermi or fermi-bose mixtures). Such van der Waals interaction in the interface of a heterostructure system also provides a possible formation of the polaron[21] in the atomic layer stacking system[20] which favors more the van der Waals interaction. Besides the van der Waals force, the attractive potential (of impurity) mediated by the crystal phonon forms the Cooper parts that produced the superconductivity phenomenon.

The fermi polaron formed in solid state is stable in weak coupling regime, and can be treated uncoupled with the environment, that is similar to the bare pairing in closed channel[23] which has higher energy than the open one (dressed), but in gaseous systems where the interaction can be turned via a magnetic field-induced Feshbach resonance, the single channel description with zero-range potential fails in weak interaction regime[22]. The properties of the polaron is closely related to the dispersion of the majority component in the bath, for the most common kind of the polaron in solid system—the electron-phonon coupling induced Bose polaron, since the dispersion of longitudinal acoustic phonon is $\sim v_s q'$ (q' is the phonon momentum) with sound velocity v_s (see, e.g., Ref.[24]).

The validity of one-particle-hole ansatz[1] in dealing with the polaron problem in the presence of many-body effect has been verified. However, according to Ref.[25], this validity requires the nearly perfect destructive interference of the contributions from other particle-hole excitations (brings the higher order terms) apart from the formed polaron, in the polaron ground state as a superpositions of the coherent many-body states. However, such a coherence requires the quantum system isolated from the environment, like a isolated impurity interact with the thermal bath or the solid medium (see Ref.[29] and the references therein). One another excellent experimental platform for the preparation of coherence is the cold atomic gases. Although the long-range coherence will destroyed by the temperature fluctuation[33], the short-range one can be observed even at room temperature[32]. While in the extreme case which with a very light impurity immersed into a bath of heavy particles, the decoherence process may happen[32]. Besides, for mobile impurity in a superfluid state (created by a degenerate Bose gas) moves slower than the speed of sound in condensate which is about 1.33×10^{-4} m/s (the speed of sound in condensate is $\sim 10^{-3}$ m/s[30]), or for the mobile impurity in a BEC which has been accelerated above the speed of sound[31] where the decoherence occur, the Bose polaron can be formed. In the latter case where the formation of polaron is usually related to the quenching dynamics at zero-temperature limit, since the interference patterns of the coherent states are destroyed and the superposition turns into the statistical mixture, it can be represented by the statistical functions and the overlap between the impurity with the majority component. In condensate, the speed of sound is proportional to the intraspecies coupling $g_{\phi\phi}$, and thus inversely proportional to the healing length which reads $\ell = 1/\sqrt{8\pi a_{\phi\phi} n}$ (n is the condensate density). The healing length here is comparable to the size of the screening cloud around the impurity (can be atom, electron, or ion). In the extreme case of strong intraspecies interaction with the leading instability (e.g., when close to the Feshbach resonance), due to the vanishing healing length, the dispersion of the Bosons (the phonon) in the presence of polaron and the effect of potential could be still similar to the above-mentioned one $\sim sk$ (s here is the speed of sound $s = \hbar/\sqrt{2m_{\phi}\ell}$ which becomes very large now; like the Debye model in metal). For the optical lattice as a two-dimensional artificial solid state system with continuous symmetry, the healing length is very small due to the harmonic transverse confinement, and thus leads to a larger speed of sound than that in the quantum gases. And specially, for two-dimensional system, the intraspecies atomic interaction decreases with the increasing oscillator length[34]. Compared to the graphene-like two-dimensional Dirac materials, the ultracold atomic system in a hexagonal (or triangular) optical lattice provides a more controllable and clean (without the impurity or defect unless added by the additional laser or magnetic field) platform to probe the polaron behavior as well as the self-trapping of the mobile impurity in equilibrium or nonequilibrium cases[35, 36].

3 Polaron model involving boson-impurity and electron-electron interactions

For composite polaron state which contains both the interactions between impurity and the induced particle-hole excitation, and that between impurity and phonon (Peierls electron-phonon interaction[72]), we can write the many-body Hamiltonian as

$$\begin{aligned}
H = & \sum_k \varepsilon_{k\uparrow} c_{k\uparrow}^\dagger c_{k\uparrow} + \sum_p \varepsilon_{p\downarrow} c_{p\downarrow}^\dagger c_{p\downarrow} + \frac{1}{N} \sum_{k,p,q} g_q c_{p-q\downarrow}^\dagger c_{k+q\uparrow}^\dagger c_{k\uparrow} c_{p\downarrow} \\
& + \sum_{q'} \Omega_{ph}^0(q') b_{q'}^\dagger b_{q'} + \frac{1}{\sqrt{N}} \sum_{p,k,q',\sigma} |g_{k+q',k}| c_{p+q',\sigma}^\dagger c_{p,\sigma} (b_{-q'}^\dagger + b_{q'}),
\end{aligned} \tag{7}$$

where $N = S/s_0$ is the total number of the unit cell where S is the total area and s_0 is the area each unit cell. $g_q^{-1} = -\sum_k [E_b + \varepsilon_{k\uparrow} + \varepsilon_{k\downarrow} + W]^{-1}$. Here we have transform the position representation into momentum basis through the unitary transformation, and use the single Einstein mode of the phonon without the second-quantization. The first term shows the contribution of the bath particles, which can, in the absence of spin flipping, includes the spin degree of freedom by simply times a factor of 2. Then the ground state wave function reads (here consider the one particle-hole

pair and one phonon limit)

$$\begin{aligned}
|\psi\rangle_{FP} &= (\psi_0 c_{p\downarrow}^\dagger + \sum_{k>k_F, q<k_F} \psi_{kq} c_{p+q-k\downarrow}^\dagger c_{k\uparrow}^\dagger c_{q\uparrow}) |0\rangle_\uparrow, \\
|\psi\rangle_{CP} &= (\phi'_0 c_{p\downarrow}^\dagger + \sum_{k>k_F, q<k_F} \phi'_{kq} c_{p+q-k\downarrow}^\dagger c_{k\uparrow}^\dagger c_{q\uparrow} + \sum_{|q'|\leq q_D} \phi_{q'} b_{-q'}^\dagger c_{p-(-q')\downarrow}^\dagger \\
&\quad + \sum_{k>k_F, q<k_F, |q'|\leq q_D} \phi_{kq q'} c_{p+q-k-(-q')\downarrow}^\dagger c_{k\uparrow}^\dagger c_{q\uparrow} b_{-q'}^\dagger) |0\rangle,
\end{aligned} \tag{8}$$

where $|\psi\rangle_{FP}$ and $|\psi\rangle_{CP}$ denote the ground state wave function of the fermi polaron and composite polaron. Here q_D denotes the Debye radiu. For the wave function $|\psi\rangle_{CP}$, we ignore the coupling between the phonons and the electron-hole pair (with total momentum $k - q$) since we assume the binding energy within the electron-hole pair (especially for the light-excited one) is much larger than that between impurity and the phonons, that is in consideration of the large exciton binding energy which could be as large as 0.3 eV in the π -conjugated system[74] or 0.5 eV in the semiconductor[67], while that of the electron-phonon polaron is only 0.3 meV in a continuum model[68], or 70 meV when consider the optical phonon[66]. For some other materials like the MoS₂, several types of excitons can be found[130], and the binding energy is dependent of the separation between atomic sites and the dielectric constant. We note that such binding energy can be reduced by the screening from fermi liquid or the band gap effect. For the composite polaron, by minimizing $\langle\psi|E - H|\psi\rangle$, we have (considering the case that emits a phonon)

$$\begin{aligned}
\langle\psi_{CP}|E_\downarrow - H|\psi_{CP}\rangle &= E_\downarrow (|\phi'_0|^2 + \sum_{kq} |\phi_{kq}|^2 + \sum_{q'} |\phi_{q'}|^2 + \sum_{kqq'} |\phi_{kqq'}|^2) \\
&\quad - [|\phi'_0|^2 \varepsilon_{p\downarrow} + \sum_{kq} (\varepsilon_{p+q-k\downarrow} + \varepsilon_{k\uparrow} - \varepsilon_{q\downarrow}) |\phi_{kq}|^2 \\
&\quad + \sum_{q'} (\varepsilon_{p-(-q')\downarrow} + \varepsilon_{-q'}) |\phi_{q'}|^2 + \sum_{kqq'} (\varepsilon_{p+q-k-(-q')} + \varepsilon_{k\uparrow} - \varepsilon_{q\uparrow} + \Omega_{ph}^0(q')) |\phi_{kqq'}|^2 \\
&\quad + |\phi'_0|^2 \sum_q g_q + \sum_{kq} (\phi_0'^* \phi_{kq} g_{k-q} + c.c.) + \sum_{q'} (\phi_0'^* \phi_{q'} g_{-q'} + c.c.) \\
&\quad + \sum_{kqq'} (\phi_0'^* \phi_{kqq'} g_{k-q+(-q')} + c.c.) \\
&\quad + \sum_{kqq'} (\phi_{kq}'^* \phi_{q'} g_{k-q+(-q')} + c.c.) + \sum_{kqq'} (\phi_{kq}'^* \phi_{kqq'} g_{q'} + c.c.) + \sum_{kqq'} (\phi_{kq}'^* \phi_{kqq'} g_{k-q} + c.c.)].
\end{aligned} \tag{9}$$

Here we ignore the change of the momentum of electron-hole pair. Then for $\frac{\partial\langle\psi_{CP}|H|\psi_{CP}\rangle}{\partial\phi} = 0$, we write

$$\begin{aligned}
\varepsilon_{p\downarrow} \phi_0 + \phi_0 \sum_q g_q + \sum_{kq} \phi_{kq} g_{k-q} + \sum_{q'} \phi_{q'} g_{-q'} + \sum_{kqq'} \phi_{kqq'} g_{k-q+(-q')} &= E \phi_0, \\
(\varepsilon_{p+q-k\downarrow} + \varepsilon_{k\uparrow} - \varepsilon_{q\downarrow}) \phi_{kq} + \phi_0 g_{k-q} + \sum_{kqq'} \phi_{q'} g_{k-q+(-q')} + \sum_{kqq'} \phi_{kqq'} g_{-q'} &= E \phi_{kq}, \\
(\varepsilon_{p-(-q')\downarrow} + \varepsilon_{-q'}) \phi_{q'} + \phi_0 g_{-q'} + \sum_{kqq'} \phi_{kq} g_{k-q+(-q')} + \sum_{kqq'} \phi_{kqq'} g_{k-q} &= E \phi_{q'}, \\
(\varepsilon_{p+q-k-(-q')} + \varepsilon_{k\uparrow} - \varepsilon_{q\uparrow} + \Omega_{ph}^0(q')) \phi_{kqq'} + \phi_0 g_{k-q+(-q')} + \sum_{kqq'} \phi_{kq} g_{-q'} + \sum_{kqq'} \phi_{q'} g_{k-q} &= E \phi_{kqq'},
\end{aligned} \tag{10}$$

The variational paramters are obtained by the minimization as

$$\begin{aligned}
\phi_0 &= \frac{\frac{g}{N} \sum_q \chi_q}{E_\downarrow - \varepsilon_{p\downarrow}}, \\
\phi_{kq} &= \frac{\frac{g}{N} \chi_q}{E_\downarrow - (\varepsilon_{p+k-q\downarrow} + \varepsilon_{k\uparrow} - \varepsilon_{q\downarrow})}, \\
\phi_{q'} &= \frac{\frac{g}{N} \sum_q \chi_q}{E_\downarrow - (\varepsilon_{p-(-q')\downarrow} + \Omega_{ph}^0(-q'))}, \\
\phi_{kqq'} &= \frac{\frac{g}{N} \chi_q}{E_\downarrow - (\varepsilon_{p+k-q-(-q')\downarrow} + \varepsilon_{k\uparrow} - \varepsilon_{q\uparrow} + \Omega_{ph}^0(-q'))}, \\
\chi_q &= \psi_0 + \sum_k \psi_{kq} + \sum_{q'} \psi_{q'} + \sum_{kq'} \psi_{kqq'},
\end{aligned} \tag{11}$$

where the self-consistent energy term ($E - \varepsilon_{p\downarrow}$) reads

$$E - \varepsilon_{p\downarrow} = \frac{1}{N} \sum_{q<k_F} \left[g^{-1} - \frac{1}{N} \sum_{k=k_F}^\Lambda \frac{1}{E + i0 - (\varepsilon_{p+k-q-(-q')\downarrow} + \varepsilon_{k\uparrow} - \varepsilon_{q\downarrow} + \Omega_{ph}^0(-q'))} \right]^{-1}, \tag{12}$$

which equals the binding energy when $p = 0$. Note that in effective mass approximation we also have $\text{Re}[\Sigma_e(\omega, p) + \Pi_e(p)] = E - \varepsilon_{p\downarrow}$. For small electron chemical potential, we define

$$g^{-1}(\Lambda) = -\frac{1}{N} \sum_{k, q'}^{\Lambda} \frac{1}{E_b + \varepsilon_{k\uparrow} + \varepsilon_{k\downarrow} + \Omega_{ph}^0(-q') + W}. \quad (13)$$

Unlike the renormalized coupling parameter in Eq.(6), we can see that this coupling parameter depends on both the binding-energy E_b and momentum (ultraviolet) cutoff Λ . and the logarithmically diverges of $g^{-1}(\Lambda) = -\infty$ can be seen ($g(\Lambda) \rightarrow 0^-$) when $\Lambda \rightarrow \infty$ (where the quantum correction vanishes). The normalization condition is ${}_{CP}\langle\psi|\psi\rangle_{CP} = |\phi_0|^2 + \sum_{k>k_F, q<k_F} |\phi_{kq}|^2 + \sum_{q'\leq q_D} |\phi_{q'}|^2 + \sum_{k>k_F, q<k_F, |q'|\leq q_D} |\phi_{kqq'}|^2 = 1$. Note that such a composite polaron cannot found in a superfluid bath since in this case the propagating impurity will not excites the electron-hole excitation. The binding energy E_b here is positive for attractive potential, i.e., the fermi polaron here with negative g_q , thus the energy of such a bound state must be negative $-E_b < 0$, which corresponds to the negative self-energy of the attractive fermi polaron.

For an analysis, we approximately suppose that there only exist two possibilities: isolate impurity or interaction with both the electron-hole pair and the phonons. Then the variational wave function reads (here consider the one particle-hole pair and multi-phonon case)

$$|\psi\rangle_{CP} = (\phi'_0 c_{p\downarrow}^\dagger + \sqrt{N_{ph}} \sum_{k>k_F, q<k_F, |q'|\leq q_D} \phi_{kqq'} c_{p+q-k-(-q')\downarrow}^\dagger c_{k\uparrow}^\dagger c_{q\uparrow}^\dagger b_{-q'}^\dagger) |0\rangle, \quad (14)$$

where the factor $\sqrt{N_{ph}}$ resulted by the $b_{-q'}$ acting on the unperturbed state $|0\rangle$. Unlike the anharmonic phonon modes induced by the high intensity laser[71, 93, 62] where the interphonons coupling can not be ignored, we ignore the interphonons coupling here as the modes are created by the self-induced lattice polarization. The residue Z will not affected largely by this approximation since the penetration length (coherence length) of the 2D system here (e.g., the tight-binding model) or the optical lattice which with deep trapping potential, are much shorter[94] than the ideal BEC[91]. The variational parameters are obtained by the minimization as

$$\begin{aligned} \phi_0 &= \frac{g N_{ph} \sum_q \chi_q}{E_\downarrow - \varepsilon_{p\downarrow}} = \frac{g n_{ph} \sum_q \chi_q}{E_\downarrow - \varepsilon_{p\downarrow}}, \\ \phi_{kqq'} &= \frac{\frac{g}{N} \chi_q}{E_\downarrow - (\varepsilon_{p+k-q-(-q')\downarrow} + \varepsilon_{k\uparrow} - \varepsilon_{q\uparrow} + \Omega_{ph}^0(-q'))}, \\ \chi_q &= \psi_0 + \sum_{kq'} \psi_{kqq'}, \end{aligned} \quad (15)$$

where n_{ph} denotes the phonon density. The normalization condition is ${}_{CP}\langle\psi|\psi\rangle_{CP} = |\phi_0|^2 + N_{ph} \sum_{k>k_F, q<k_F, |q'|\leq q_D} |\phi_{kqq'}|^2 = 1$. Here the momentum distribution of polaron is shifted from the δ_p -function by the electron-phonon coupling term $|\phi_{kqq'}|^2$. Through the above procedure, we can obtain

$$\begin{aligned} \frac{\phi_{kqq'}}{\phi_0} &= \frac{g \frac{1}{N} \chi_q (E - \varepsilon_{p\downarrow})}{g \frac{N_{ph}}{N} \sum_q \chi_q (E - (\varepsilon_{p+k-q-(-q')\downarrow} + \varepsilon_{k\uparrow} - \varepsilon_{q\uparrow} + \Omega_{ph}^0(-q')))} \\ &= \frac{1}{N_{ph} N} \frac{E - \varepsilon_{p\downarrow}}{E - (\varepsilon_{p+k-q-(-q')\downarrow} + \varepsilon_{k\uparrow} - \varepsilon_{q\uparrow} + \Omega_{ph}^0(-q'))}, \end{aligned} \quad (16)$$

where the energy is

$$\begin{aligned} E - \varepsilon_{p\downarrow} &= \frac{1}{N} \sum_{q<k_F} \left[g^{-1} - \frac{1}{N} \sum_{k=k_F}^{\Lambda} \frac{1}{E + i0 - (\varepsilon_{p+k-q-(-q')\downarrow} + \varepsilon_{k\uparrow} - \varepsilon_{q\uparrow} + N_{ph} \Omega_{ph}^0(-q'))} \right]^{-1}, \\ &= \frac{1}{N} \sum_{q<k_F} \left[-\frac{1}{N} \sum_{k, q'}^{\Lambda} \frac{1}{E_b + \varepsilon_{k\uparrow} + \varepsilon_{k\downarrow} + N_{ph} \Omega_{ph}^0(-q')} \right. \\ &\quad \left. - \frac{1}{N} \sum_{k=k_F, q'}^{\Lambda} \frac{1}{E + i0 - (\varepsilon_{p+k-q-(-q')\downarrow} + \varepsilon_{k\uparrow} - \varepsilon_{q\uparrow} + N_{ph} \Omega_{ph}^0(-q'))} \right]^{-1}. \end{aligned} \quad (17)$$

Note that for the majority component, the eigenenergy should contains the chemical potential, e.g., in above equation we have $\varepsilon_{k\uparrow} = \frac{k^2}{2m_\uparrow} - \mu_\uparrow$ and $\varepsilon_{q\uparrow} = \frac{q^2}{2m_\uparrow} + \mu_\uparrow$, i.e., the pair energy is measured from $2\mu_\uparrow$.

4 Electron-phonon coupling

4.1 Polaronic effect induced by electron-phonon coupling (boson-impurity interaction)

The transition of the quasifree polaron (large size) to the self-trapped polaron (small size) could be realized for solid state system in strong coupling region. Similar to the Fröhlich Hamiltonian[37], in solid state, the electron-phonon coupling can be described by the approximation up to first order of the atomic displacements. We at first discuss the weak coupling adiabatic case, where the Migdal-Eliashberg theory is applicable, then the (single species) self-energy of the phonon (no matter transverse or longitudinal modes) can be obtained by the summation of the electronic states (excited by the electron-phonon interaction) with different crystal momenta during the transition

$$\Sigma_{ph}(q', \Omega_{ph}) = \int \frac{d^2k}{(2\pi)^2} |g_{p,p+q'}|^2 \frac{N_F(\varepsilon_{k+q'}) - N_F(\varepsilon_k)}{\varepsilon_{k+q'} - \varepsilon_{q'} - \Omega_{ph} - i0}, \quad (18)$$

where $g_{p,p+q'}$ is the well known electron-phonon coupling matrix element[38, 39, 132, 41, 42] which is inversely proportional to the atomic mass and the bare phonon frequency $\Omega_{ph}^0(q')$, just similar to the descriptions in collective Holstein approximation. We have in perturbational treatment

$$g_{p,p+q'} = \sqrt{\frac{\hbar}{2M\Omega_{ph}^0}} \langle k+q' | \frac{\delta U}{\delta u_q} | k \rangle, \quad (19)$$

where M is the atomic mass of the lattice and δU is the variation of the self-consistent Kohn-Sham potential. δu_q denotes the tight-binding amplitude. Here the change of quantum numbers are not shown which make the self-energy nonzero even in the limit $q' \rightarrow 0$. We can see that this self-energy is just the polarization loop (particle-hole bubble) with the crossing phonon vertex correction. Note that in Migdal approximation, the effect of phonon vertex correction is small and even negligible[43] due to the weak electron-phonon coupling strength (compared to the electron tunneling), $\varepsilon_{e-ph} (\sim |g_{p,p+q'}|^2) \ll 3t\Omega_{ph}$ ($3t$ here is the approximated bare half bandwidth of a two-dimensional honeycomb lattice system, which is 8.4 eV in the intrinsic graphene; for large polaron, the half bandwidth can also be written as $\frac{3}{2ma^2}$ [76]), in which case the effective mass of electron ($m^* = m(1 + \frac{\varepsilon_{e-ph}}{3t\Omega_{ph}^0})$) is closes to the rest one. Note that the above phonon self-energy induced by the propagating electron is valid only within the Migdal-Eliashberg approximation, i.e., the weakly coupled adiabatic limit $\frac{\varepsilon_{e-ph}}{3t\Omega_{ph}^0} \ll 1$, $\frac{t}{\Omega_{ph}^0(q')} \ll 1$. (In the insulator phase with large electron-phonon coupling, the Migdal-Eliashberg approximation breaks down) The real part of above phonon self-energy provides the phonon frequency shift while its imaginary part provides the phonon linewidth (or the population decay[61]) since it does not contains the phonon-related vertex correction. The phonon linewidth is proportional to the electron-phonon coupling matrix element and inversely proportional to the fermi velocity of electron, i.e., the self-energy will induces a higher linewidth in nonadiabatic case, in other word, the linewidth increases with the increase of doping level. Note that here the contributions to linewidth from the anharmonic term (inter-phonon interaction) and the interaction between phonons and the electron-hole pairs are neglected.

As diagrammatically shown in the Fig.1, the boson self-energy loop (phonon) obtained by many-body diagrammatic method is comprised of two fermion propagators (the impurity) and two boson propagators (with external momentum and external frequency) where we consider the current-current correlation here. The phonon vertex correction reads

$$\sigma_j \Gamma_{ph} = \sigma_j - \sum_{q', \Omega_{ph}} TD_{ph}(q', \Omega_{ph}) |g_{k,k+q}|^2 G_0(k+q', \omega + \Omega_{ph}) \sigma_j' \Gamma_{ph}' G_0(k+q+q', \omega + \Omega + \Omega_{ph}), \quad (20)$$

where ω is the fermion frequency and Ω/Ω_{ph} is the bosonic frequency. Here the Pauli matrices σ can also be replaced by the Dirac γ matrices[44, 127], which then requires a new form of Dirac quasiparticle propagator. In the weak-coupling region, $D_{ph}^0(q', \Omega_{ph}) = \frac{2\Omega_{ph}^0(q')}{\Omega_{ph}^2 - \Omega_{ph}^0(q')}$ is the bare phonon propagator, which should be replaced by the interacting one when the electron-phonon coupling is strong (and thus with a larger phonon self-energy):

$$D_{ph}(q', \Omega_{ph}) = \frac{2\tilde{\Omega}_{ph}^0(q')}{\Omega_{ph}^2 - \tilde{\Omega}_{ph}^0(q') - 2\tilde{\Omega}_{ph}^0(q')\Sigma_{ph}(q', \Omega_{ph})} \quad (21)$$

where $\tilde{\Omega}_{ph}^0 = \Omega_{ph}^0(q')(1 - 2\frac{\varepsilon_{e-ph}}{t})$ is the renormalized phonon frequency.

For gapless band structure, the states could be adiabatically pass through the massless Dirac point no matter in Dirac material or the artificial honeycomb optical lattice [46], while for the case that the phonon energies are smaller than the band gap, the interband contributions from the excited electrons vanish, and the adiabaticity is also broken due to the crossing of the lowest bands or the large separation (larger than the phonon energy) of bands. The electron-phonon coupling matrix element can be rewritten as (for optical phonon scattering)

$$g_{p,p+q'} = g_{p,p+q'}^0 [u_{p+q',s}^* u'_{p,s'} \frac{1}{\varepsilon_p} (\mathbf{t}_p \cdot \boldsymbol{\phi}'_{q'} - \mathbf{t}_{p+q'} \cdot \boldsymbol{\phi}'_{q'}) + u_{p+q',s}^* u_{p,s'} \frac{1}{\varepsilon_p} (-\mathbf{t}_{-p} \cdot \boldsymbol{\phi}'_{q'} + \mathbf{t}_{-p-q'} \cdot \boldsymbol{\phi}'_{q'})], \quad (22)$$

with

$$g_{p,p+q'}^0 = \frac{\varepsilon_{e-ph}}{\Omega_{ph}^0} \sqrt{\frac{s_0}{M}} \approx \frac{6\hbar v_F}{a^2 \sqrt{2} \frac{2M}{s_0} \Omega_{ph}^0 S} = \frac{3\sqrt{3}t}{a\sqrt{4MN\Omega_{ph}^0}}, \quad (23)$$

where $N = S/s_0$ is the number of unit cell, and $2M$ is the atomic mass per unit cell. For optical phonon, the Ω_{ph}^0 in the denominator is the optical phonon frequency in the BZ center (Γ -point) which is independent of the dispersion. In graphene, the $g_{p,p+q'}^0$ is estimated as 5.3 eV/\AA [66]. This expression is obviously a tight-binding treatment which is in the basis of tight-binding amplitudes u , where \mathbf{t}_k is the hopping vector of the electron and ϕ is the phonon eigenvector (vibrational modes) whose direction is related to the vibrational direction. u and u' correspond to the two basis vectors. s and s' are the band indices. We can see that when the nearest-neighbor hopping direction is orthogonal to vibrational direction, the electron-phonon interaction vanishes. When the polaron-phonon interaction is ignored (like the closed channel), the hopping has a simple expression

$$\begin{aligned} t_k &= \int d\mathbf{r} w^*(\mathbf{r} - \mathbf{R}) H_0 w(\mathbf{r} - \mathbf{R}) \\ &= \frac{1}{2N} \sum_{\mathbf{R}, \delta} \varepsilon_k \delta e^{i\mathbf{k} \cdot \mathbf{R}} \end{aligned} \quad (24)$$

where $2N$ is the site number here since we assume the primitive unit cell which contains two sites, δ is the unit vector of the nearest-neighbor hopping, \mathbf{R} is the lattice vector of the primitive unit cell, H_0 is the noninteracting Hamiltonian, $w(\mathbf{r} - \mathbf{R})$ is the Wannier function which containing the Bloch eigenstates (for linear Schrodinger equation)[56, 57]. When the polaron-phonon interaction is taken into account, the self-energy of an impurity electron induced by the electron-phonon interaction is

$$\begin{aligned} \Pi_e(p) &= \int \frac{d^2 q'}{(2\pi)^2} |g_{k,k+q'}|^2 D_{ph}(q', \Omega_{ph}) G_0(p+q', \omega + \Omega_{ph}) \\ &= \int \frac{d^2 q'}{(2\pi)^2} |g_{p,p+q'}|^2 \left(\frac{1 + N_B(\Omega_{ph}^0(q'))}{\varepsilon_{p-q'} - \varepsilon_p + \Omega_{ph}^0(q') + i0} + \frac{N_B(\Omega_{ph}^0(q'))}{\varepsilon_{p+q'} - \varepsilon_p - \Omega_{ph}^0(q') + i0} \right), \end{aligned} \quad (25)$$

where the analytical continuation $i\Omega \rightarrow \Omega + i\eta^+$ is used[126, 127]. Note that the signs of imaginary part of self-energy and the spectral function (positive or negative) are dependent on the sign of infinite small quantity η . The hopping in real space needs to containing the effects of the emission or absorption of phonons, and becomes $t'_{ij} = t_{ij} \exp[\sum_{q'} \frac{|g_{p,p+q'}|}{\sqrt{N}} (c_i^\dagger c_i d_{q'} - c_j^\dagger c_j d_{q'}) - h.c.]$, which contains the effect of electron-phonon Fröhlich interaction. as described by the electron scattering (inelastic) rate, which can be obtained by the imaginary part of electron self-energy

$$\frac{1}{\tau_e} = \frac{2\pi}{\hbar} \sum_{q'} |g_{p,p+q'}|^2 [(N_B(\Omega_{ph}^0(q')) + 1)\delta(\varepsilon_{k-q'} - \varepsilon_k + \Omega_{ph}^0(q')) + N_B(\Omega_{ph}^0(q'))\delta(\varepsilon_{k+q'} - \varepsilon_k - \Omega_{ph}^0(q'))], \quad (26)$$

the two terms within the square bracket correspond to the emission and absorption of a phonon respectively, as persistently happen during the coherent propagation of the phonon (dressed by the cloud of phonons). Apparently, at zero-temperature, the scattering rate (relaxation) is related to the selection rule $\varepsilon_{k-q'} - \varepsilon_k = -\Omega_{ph}^0(q')$, and it is coupled to the self-induced lattice polarization here.

For acoustic phonon, the matrix element $|g_{p,p+q'}|^2$ in above equation should be replaced by

$$\frac{s_0}{M} \frac{D^2 q'^2}{2\Omega_{ph}^0} |\langle k + q' | k \rangle|^2 = \frac{s_0}{M} \frac{D^2 q'^2}{2\Omega_{ph}^0} \frac{1 + ss' \cos\theta}{2}, \quad (27)$$

where D is the screened (quasistatic) deformation potential, s_0 is the area of the unit cell, and θ denotes the angle between $k + q'$ and k . Note that here we discuss the case that the quasiparticle which dressed with the phonons is the fermi polaron: an electron dressed with electron-hole parts (when the electron-electron interaction (electron self energy) is taken into account). While for the BEC in hexagonal optical lattice system, the above tight-binding treatment fails to describes the modification of the band structure in Dirac cone by the interatomic interactions[46], however, we still find a common point. For both the Dirac material and honeycomb optical lattice, the adiabatic evolution of the electron eigenstates is broken when the band crossing happens, which gives rise to the nonlinearity[47]. This similarity requires the extreme low temperature in which case there are not thermally excited phonons.

For BEC in linear quantum regime, the adiabatic evolution maintains as long as the variance of the perturbation, which can simply described by the nonlinear Dirac equation with a momentum (or continuous wave function) dependent short range interaction term, is slower than the frequency (level spacing). For Dirac solid material, the electron-phonon coupling strength $|g_{p,p+q'}|^2$ changes linearly along the irreducible Brillouin zone[42] when the Dirac linear dispersion is presented or with band gap which is smaller than phonon energy Ω_{ph}^0 . This implies that $|g_{p,p+q'}|$ is independent of the electron momentum in the adiabatic case, but depends only on the exchange momentum q' . That is consistent with the strong coupling adiabatic in Holstein (lattice) model where the hopping t_k is much larger than the phonon frequency, and thus the electron transition (or tunneling) between different levels (or eigenstates) is suppressed, which leads to the exponentially reduced (collapsed) polaronic bandwidth. We note that, for the tunneling of BEC, the level crossing

between the eigenstates from valence band (but not from conduction band and valence band) can happen[46, 47, 49, 48] due to the additional eigenstates in nonlinear frame as described (at zero-temperature limit) by the Gross-Pitaevskii equation within mean-field approximation. That is not unique to the BEC in an optical lattice, the multilayer Dirac materials also have such kind of level crossing (like the bilayer graphene or bilayer silicene[50]).

4.2 Decoherence effect induced by electron-phonon coupling

Now let us temporarily return to the problem of decoherence, where the pairing instability can be described by the statistic mixture (Fermion or Bosonic distribution function) as shown in the pair propagator and the (non-self-consistent) T -matrix. For an atomic system, the occurrence of decoherence (accompanied by an exponential decay of the quasiparticle lifetime $\tau = \frac{-\text{sgn}[\Omega]}{2\text{Im}\Sigma(\Omega)}$) requires that the velocity of the impurity is faster than the speed of sound in condensate, and thus the momentum becomes larger than the Landau critical momentum. That usually happen in the extreme case of mass-imbalance between impurity and the majority particles. While in the opposite case, the superposition (coherence) mentioned in Ref.[25] is possible since they consider the case of zero impurity momentum which can be realized in a mixture where the two spin species have equal masses, such configuration has also been considered in Refs.[51, 63]. For the transition of electron states near Dirac cone, even the smallest perturbation could breaks the adiabaticity, and the nonlinear dynamics induced by the on-site interaction will breaks the superposition of states as well as the coherence and the noticeable interference patterns. Thus we conclude that, near Dirac cone, the transition of electrons is adiabatic both for the linear band structure or with a small band gap (e.g., smaller than the bare phonon energy). While in the extreme adiabatic and strong coupling case where the electron hopping amplitude is much larger than the phonon frequency (or much larger than the Bloch energy of bosons E_B , which is intraspecies interaction-dependent for a bosonic gas[53]), since in this case the velocity of impurity (the electron) in real space is much larger than the bath component, as indicated by $t \gg \Omega_{ph}^0$ and infinite bath effective mass, the coherence is decreased and the decoherence is enhanced, as exhibited by the reduction of the coherent quantum motion. And it is indeed a diffusive motion (incoherent) which also contributes to the conductivity unless when a magnetic field is applied. In this case, the impurity with large velocity will excites, e.g., the electron-hole excitations or phonons, or even emits the Cherenkov radiation, and thus the superfluid can not emergents as the impurity losses energy during this process, as observed recently of the self-trapped small polaron in haematite, where the photoexcited carriers exciting the optical phonons during the process of charge-transfer[62]. Then the polaronic band (or electron band) collapse and leads to a charged ordered insulating state as long as the zero-point quantum fluctuation is weaker than the lattice distortion. However, the self-trapping of polaron may be destroyed by the thermal fluctuation at high temperature as recently studied in Ref.[69]. Note that the charged ordered insulating state mentioned above is essentially different from the Mott insulator state where the on-site interaction strength is very large and the impurity propagation induces the coherent quantum motion. Such extreme adiabatic limit corresponds to the local phonon modes and maximal decoherence with the impurity density matrix ρ_p loses its off-diagonal elements: $c_{p+q}^\dagger c_p$ and $c_{p+q'} c_p^\dagger$. Experimentally, the hopping here can be manipulated by the magnetic gradient modulation in atomic system[60] or by the strain in a solid state system[115].

The perturbation from quantum fluctuation in a lattice system is more significant in 2D than that in the 3D, as reflected by the high-order expansion about the ratio of t/U . For most cases, like for the ultracold atomic system[32] and the Holstein compounds[109, 43], the polaronic band collapse happen as long as $\varepsilon_{e-ph}/t \gtrsim 1$, and for the former one, the linear feature of the lattice near Dirac cone requires the hopping strength (or the coupling between modes) larger than the nonlinear eigenvalue which forms the Bloch bands $t > N g_{\psi\psi} \mathcal{Z}_\psi \rightarrow 0$, where N is the particle number, $g_{\psi\psi}$ is the electron-electron interaction (characterized by the s -wave interaction), and \mathcal{Z}_ψ is the probability of a electron to be interacting. On the other hand, when the band crossing happen, like the overlap between conduction band and valence band or the loop structure which emerges in the lowest Bloch band as obtained by the eigenvalues of the tight-binding Hamiltonian (or nonlinear Dirac equation) and the nonlinear Schrodinger equation, respectively, the superconductivity[50] or superfluidity[46, 54, 55] can be observed, as the strong short-range interaction (the deformation potential-independent one) can helps the plane wave to overcomes the perturbations (like the periodic potential of optical lattice or the lattice defect). As an example, the bipolarons formed in real space, which requires strong enough impurity-impurity interaction[28], are with highly nonadiabatic charectes in real space, which results in a different superconducting[59] mechanism compared to the BCS one.

We note that, the electron-phonon coupling term $\frac{\varepsilon_{e-ph}}{3t\Omega_{ph}^0(q')}$ obtained above is base on the combination of the polaron energy shift in single-site frame, i.e., assume the hopping is $t = 0$ like in the atomic limit, and the finite bandwidth. Usually, this description of coupling is valid in the tight-binding model as well as the orthorhombic YBCO compounds. The effect of hopping becomes dominative when the size of polaron is smaller than the lattice spacing, as described by the tight-binding Hamiltonian, and the value of hopping determines the dispersion of the mode and the motion (velocity) of the impurity. For slow motion, the decay rate of the polaron (as a quasiparticle) decreases and vanishes at long-time limit. then leads to the negative polaron self-energy, i.e., the attractive polaron[64, 1, 5].

5 Self-energy effects, effective mass and residue of impurity due to the interaction with acoustic phonon and particle-hole pair

The induced effective mass can be written as $\Delta m^* = -[\frac{\partial^2 E(p)}{\partial p^2}]^{-1} = [\frac{\partial^2 |E(p)|}{\partial p^2}]^{-1}$. For the case that the dispersion of polaron is nearly quadratic, the following approximated expression is valid[19]

$$\begin{aligned}\Delta m^* &= \frac{p}{\partial_p E(p)} = \frac{1}{\frac{1}{m_\downarrow} + \frac{1}{p} \partial_p \text{Re}[\Sigma(E(p), p)]|_{E(p)}} \\ &= \frac{1/Z}{\frac{1}{m_\downarrow} + \frac{1}{p} \partial_p \text{Re}[\Sigma_e(\omega, p) + \Pi_e(p)]|_{E(p)}},\end{aligned}\quad (28)$$

where the second line of above expression corresponds to the linear expansion around the pole (quasienergy) of the impurity Green's function.

The quasiparticle residue (spectral weight) Z is given by the GW calculation result

$$\begin{aligned}Z^{-1} &\equiv 1 - \partial_\omega \text{Re}[\Sigma_e(\omega, p) + \Pi_e(p)]|_{\omega=E(p)} \\ &= |\phi_0|^{-2} = 1 + \sum_{k > k_F, q < k_F, |q'| \leq q_D} \left(\frac{\phi_{kqq'}}{\phi_0}\right)^2 \\ &\approx 1 + \frac{1}{N_{ph}} (Z_{\min}^{-1} - \frac{E - \varepsilon_{p\downarrow}}{2N_{ph}\tilde{g}} - 1).\end{aligned}\quad (29)$$

Note that here $E(p) = \varepsilon_{p\downarrow} + \text{Re}\Sigma(\omega, p)$ is the pole of the impurity Green's function $G(\omega, p) = 1/(\omega + i0 - \varepsilon_{p\downarrow} - \text{Re}\Sigma(\omega, p))$, which can be rewritten as the dressed impurity propagator: $G(\omega, p) = Z/(\omega + i\gamma - \varepsilon_{p\downarrow} - \text{Re}\Sigma(E(p), p))$, where $\gamma = -Z\text{Im}\Sigma = -Z(\frac{-1}{2\tau})\text{sgn}(\omega)$. In the third line of above equation, we use the approximated formula, where \tilde{g} is the renormalized coupling parameter, $\tilde{g}^{-1} = g^{-1} + \frac{1}{N} \sum_{k, q'} \frac{1}{\varepsilon_{k\uparrow + \varepsilon_{k\downarrow} + \Omega_{ph}^0(-q') + W}$, which is comparable with the mean-field

polaron energy. In single phonon limit, it reduced to $Z^{-1} \approx Z_{\min}^{-1} - \frac{E - \varepsilon_{p\downarrow}}{2\tilde{g}}$, which means Z^{-1} decreases with the raising self-consistent polaron energy $E - \varepsilon_{p\downarrow}$. Similar result is obtained for organic semiconductor[104]. The Z_{\min} here is the minimal value of the quasiparticle residue of the 2D solid system, which is generally larger than that of the ultracold fermi degenerate gases (0.39)[95] or the bose gases (0.67)[99], for example, the electron residue measured in semiconductors is 0.74[104]. That is partly due to the effect of linear dispersion in the presence of Dirac or Weyl cones (undoped semimetal) with the broken down Fermi-liquid picture, where the ratio of (long-ranged) Coulomb potential to the kinetic energy, $e^2/\hbar v_F \epsilon$ (the effective fine structure constant[100, 101], where ϵ here is the environment dielectric constant), becomes very large. The residue can even becomes zero in the multi-Weyl semimetal[92] with the dressed Coulomb potential. While for the self-trapping of polaron in the Holstein model, the residue could as low as 0.1-0.2[104].

For electron self-energy induced by the electron-phonon coupling obtained above, obviously, the Eq.() is for the case of single electron, while for the many-electron case, the electron self-energy should be replaced by[65, 122]

$$\Pi_e(p) = \int \frac{d^2 q'}{(2\pi)^2} |g_{p, p+q'}|^2 \left(\frac{1 + N_B(\Omega_{ph}^0(q')) - N_F(p + q')}{\varepsilon_{p-q'} - \varepsilon_p + \Omega_{ph}^0(q') + i\eta} + \frac{N_B(\Omega_{ph}^0(q')) + N_F(p + q')}{\varepsilon_{p+q'} - \varepsilon_p - \Omega_{ph}^0(q') + i\eta} \right). \quad (30)$$

In Fan-Migdal approximation, the function N_F can be treated as a step function, which vanishes for unoccupied Kohn-Sham state[122], and the function N_B exists at finite temperature. While for adiabatic case with zero temperature, the zero-point renormalization can be obtained as $\int \frac{d^2 q'}{(2\pi)^2} |g_{p, p+q'}|^2 \frac{1}{\varepsilon_{p-q'} - \varepsilon_p}$, when the Debye-Waller term is neglected.

In long-wavelength limit, the electron-phonon coupling matrix element $\frac{D^2 \hbar q^2 s_0}{2M\Omega_{ph}} (1 - \frac{q'^2}{p^2}) \frac{1 + s s' \cos\theta}{2}$ can be reduced as $\frac{D^2 \hbar q^2 s_0}{2M\Omega_{ph}}$. For the two-dimensional materials which with linear transverse acoustic (TA) and longitudinal acoustic (LA) phonon dispersion in small- q' region, we can write $\Omega_{ph}^0(q') = v_s q'$ where $v_s = v_L (v_T)$ is the sound velocity of the LA mode (TA mode). For simulation, we set $v_L = 1.6v_{TA}$, which is applicable for graphene, silicene, blue phosphorene, and MoS₂ according to the DFT based calculation results[24, 38]. While for out-of-plane (flexural) acoustic phonon (ZA) which is closely related to the thermal conductivity of the crystal lattice[121], the disperion can be approximately written as q'^α with $\alpha \geq 2$. In the following, we at first set $\alpha = 2$.

Fig.2 shows the self-energy and effective masses of the polaron induced by the electron-phonon coupling. The real-part of the self-energy $\Pi_e(p)$ corresponds to the energy shift of the impurity, which gives rise to the renormalization effect to the intrinsic impurity dispersion. From the real part of the self-energy, we can see that there exist kinks (for TA and LA modes) or discontinuity (for ZA mode) in their first derivative, and the coordinates for these kinks or discontinuity are dependent on the sound velocity of the corresponding mode, e.g., we can see these special points are local on $p = 1$ and $p = 1.6$ (since we set the impurity mass as $m = 1$). The imaginary part of the self-energy (also related to the impurity scattering rate and the coherence length) also shows the sound velocity-dependence: The polaronic instability does not emerges until the velocity of impurity is larger than the speed of sound. We will find that the induced effective masses also obey this rule, i.e., the induced effective masses (calculated by using the exact expression) becomes nonzero only when the impurity moves faster than the sound velocity (in other words, when the momentum of impurity is larger than

the Landau critical momentum $v_s p$), and we know that the decoherence effect only emerges in this case. The induced effective masses exhibit a power-law dependence on the momentum p (with a exponent larger than one). In the last panel, we compare the results of the induced effective masses calculated by the exact expression (blue and red lines) and approximated expression (green and black lines) for TA and LA phonons. We can see that the approximated expression of the induced effective mass loss its accuracy in such case, which reveals great difference in polaronic dynamics in solid state system (crystal lattice) compared to the one in the BEC and atomic lattice system[19].

Here we focus only on the low-energy case, while in the presence of high field, the impurity scattering rate contributed by the optical phonons. Also, the strong binding due to the optical phonon-electron coupling will give rise to large polaronic energy shift[66] as well as the band gap renormalization (the band gap is reduced since the binding energy here is positive and the induced bound state energy is negative). Certainly, that requires much higher temperature to realize the optical excitation, for example, at 600 K or even 1600 K as reported in Ref.[62], in which case the acoustic phonons would not be expected to directly participate the polaron formation. Another important difference is that at high temperatures the distribution of electrons (in multi-impurity case) and phonons obey the Maxwell-Boltzmann law. This is also verified by the DFT result[71] that the high intensity laser-induced phonon-phonon interaction cannot be well described by the usual polarization formula[70] which contains two Dirac-Fermi distribution functions for electron and hole respectively. In Fig.3, we show the spectral function GW calculation. We can see that, in the stable region ($p > 0.6$) where $\text{Im}\Pi_e(p) \rightarrow 0$ (see Fig.2), the rebuilt polaron band (by the electron-phonon coupling) is linear with the momentum, while in the unstable region, we can clearly see that the polaronic mode is damped, then the damping dynamical could be described by the Landau theory when the Fermi liquid picture is preserved. For linear phonon mode, the induced polaronic mode does not damped for static polaron ($p = 0$), as can be seen from the bright spots which form the high order dispersion. Note that the dispersion showed here is not the final polaron dispersion, but just exhibits the effect of self-energy (electron-phonon coupling) to the original impurity dispersion (which is simply quadratic for the free electron occupying the surface of 2D system we discussing). We can also see that the slope of linear dispersion for q'^2 -phonon is smaller than the linear acoustic phonon.

Similarly, for $\Omega_{ph}^0 \sim q'^4$ ($\alpha = 4$), we obtain

$$\begin{aligned} \Pi_e(p) = & \frac{D^2 s_0}{4\pi M} \frac{1}{2i\eta} \left(-((2\hbar^2 p \arctan[\frac{(2mq + \hbar^2(-p+q))}{\sqrt{B}}])/\sqrt{B}) - 2\ln q \right. \\ & \left. + \ln(\hbar^2 q(-2p+q) + 2m(q^2 - iz)) \right) \Big|_{q'}, \end{aligned} \quad (31)$$

where $B = -\hbar^4 p^2 - 2\hbar^2 m i \eta - 4m^2 i \eta$. For finite (low) temperature where the distribution of phonon still obeys the Bose-Einstein one, we obtain

$$\begin{aligned} \Pi_e(p) = & \frac{D^2 s_0}{4\pi M} \frac{1}{(2b^2 i \eta \sqrt{A})} \\ & (2(-\hbar^2 p T + \beta m(T + 2i\eta)) \arctan[\frac{(\beta m + \hbar^2(-p+q))}{\sqrt{A}}]) \\ & + T((-2\beta m + 2\hbar^2 p) \arctan[\frac{(-\beta m + \hbar^2(p+q))}{\sqrt{A}}]) \\ & + \sqrt{A}(-4\ln(q) + \ln(2\beta m q + \hbar^2 q(-2p+q) - 2im\eta) + \ln(-2\beta m q + \hbar^2 q(2p+q) - 2im\eta))) \Big|_{q'}, \end{aligned} \quad (32)$$

Note that although we focus on the long-wave limit of q' , the detail integrate range of q' depends on the setting of the temperature. Our results are in agree with Ref.[66] that in low-energy limit the self-energy is heavily affected by the change of the temperature, thus we select the not-too-small value of q' for better understanding. That can also be explained by the failure of RPA when the Fermi energy is smaller than or just comparable with the phonon frequency (temperature-dependent), and the above expression of electron self-energy becomes unphysical when $\Omega_{ph}^0(q') = 0$ in the denominator. From Fig.2 and Fig.4, we can see that the self-energy of impurity electron dressed by phonon could is not totally negative, which suggest that the interaction between the electron and phonons (acoustic or the breathing-mode one) could be attractive or repulsive. That is different with the normal attractive Fermi polaron[25].

While for the Fermi polaron formed by the excited electron-hole pair, the self-energy of the impurity obtained by the method of non-self-consistent T -matrix can be written as (at zero-temperature limit)

$$\begin{aligned} \Sigma_e(p, \omega) = & \int \frac{d^2 q}{(2\pi)^2} T(p+q, \omega + \nu_q) \\ = & \int \frac{d^2 q}{(2\pi)^2} [g_q^{-1} - L(p+q, \omega + \nu_q)]^{-1} \\ = & \int \frac{d^2 q}{(2\pi)^2} \left[g_q^{-1} - \int_{k_F}^{\Lambda} \frac{d^2 k}{(2\pi)^2} \frac{1}{\omega + i\eta - \varepsilon_{p+q-k\downarrow} - \varepsilon_{k\uparrow} + \varepsilon_{q\uparrow}} \right]^{-1}, \end{aligned} \quad (33)$$

where ω and ν_q are the impurity and hole frequency, respectively. Within the expression of bare coupling g^{-1} (see Eq.()), we use the polaron shift in a single site (i.e., in zero tunneling limit and $p = 0$) instead of the binding energy of the

bounded state which is $E_b = \min\langle\psi_{CP}|E - \varepsilon_{p=0\downarrow}|\psi\rangle_{CP} = \hbar^2/2m_r a_{\phi\psi}^2$ (m_r is the reduced mass and $a_{\phi\psi}$ is the interspecies scattering length), i.e.,

$$\frac{1}{g} = -\frac{1}{N} \sum_k^\Lambda \frac{1}{\frac{g^2}{2m_{e-h}\omega_{e-h}^2} + \varepsilon_{k\uparrow} + \varepsilon_{k\downarrow} + W}, \quad (34)$$

where g is the interaction vertex between the impurity and the electron-hole pair, m_{e-h} and ω_{e-h} are the mass and frequency of the electron-hole pair. Here the summation over electron momentum k can be replaced by in continuum limit through the relation $\frac{1}{N}\Sigma = \int \frac{d\mathbf{q}}{\Omega}$ (Ω is the BZ area). Obviously, the self-energy of this Fermi polaron depends on both the impurity momentum and frequency, i.e., it is related to the response to the effective electric field.

Fig.4 shows the self-energy, effective mass, and the spectral function of the fermi polaron at different impurity frequency ω . From the expression given above, we can know that the self-energy of fermi polaron is directly related to the coupling constant g^{-1} . From the third panel of Fig.4, we can see that the induced effective mass has a difference compared to the bose polaron one: For $\omega = 2$, the induced effective mass initially has a negative value, which means that the interaction between impurity and the electron-hole pair initially reduce the effective mass of polaron and thus makes it moves faster. But in large momentum region, the tendency of induced effective mass is the same as the bose polaron one. The induced effective masses here are calculated through the exact expression $\Delta m^* = \frac{\partial^2 |E(p)|}{\partial p^2}$. Here we only present the results for the bare coupling $g_b = -0.5$, but by changing the value of g_b , we obtain that the real part of self-energy (no matter how large the ω is) at large momentum will always equal to g_b , i.e., the attractive feature of the polaron enhanced by the increasing $|g_b|$, while the induced effective masses will decrease rapidly with the increase of $|g_b|$ ($g_b < 0$). From (e), we can see that the electron spectral function ($p > 0$) is much wider than the hole spectral function ($p < 0$), and by changing the value of g_b , we find that, for positive g_b (repulsive interaction), the hole spectral function will becomes wider than the electron spectral function. In Fig.5, we present the density plot of the fermi polaron spectral function. As can be seen, the electron-hole symmetry is broken due to the different value of electron momentum k and hole momentum p , and the peaks in particle spectral function is much higher than the electron one. Our results are in agree with Fig.12-13 of Ref.[125]. Besides, for electron part of the spectral function, we can see the double-peak structure (BCS-type) like the ones found in Refs.[128, 129].

In Fig.6, the quasiparticle residue is presented. We can see that, for zero coupling constant $g = 0$ ($\Lambda \rightarrow \infty$), the residue is always equals to one, which means that there does not exists the interacting particle, and thus the polaron is absent. For $0 < g < 1$, a unusual fluctuation of residue emerges in low momentum region. We suppose such behavior is related to the singular self-energy in this momentum region. While for $g \geq 1$, the large fluctuation in residue vanishes, and we can always see a dip structure at momentum $p = 2.75$. We note that the momentum corresponds to such dip structure is independent of the coupling constant g , but it varies with the solution of the self-consistent equation (Eq.): the value of this momentum increases with the increase of polaron energy $E(p)$. At large momentum, the residue in all panels tend to one. For larger coupling g , the residue tends to one at larger momentum.

Fig.5 shows the self-energy induced by the interaction between impurity and the electron-hole pair at strong-coupling regime where the bare coupling $g(\Lambda) \rightarrow \infty$, although g^{-1} is in fact weakly depends on the relative momentum q . We can see that the sign of coupling directly affects the sign of self-energy Σ_e , and the range of negative self-energy increase with the increaseing impurity frequency. For $\omega \neq 0$, the imaginary part of self-energy (also the linewidth) has two peaks throughout the whole momentum range, that is in agree with the experimental result about the Fermi polaron as reported in Ref.[4]. While for the slow impurity in the bose polaron with momentum $p \ll \max[\mu_\uparrow, \sqrt{2m_\downarrow}\Omega_{ph}^0(q')]$, the polaron energy is purely real and thus the momentum and energy are conserved. Such stable bound state could also be found in the polaron-polaron continuum region or the bipolaron-phonon continuum region[69], where the polarons are unbounded or bounded but through emission and absorption of one phonon.

The above self-energy of impurity electron gives the second-order correction to the intrinsic electron energy, $E = \frac{\hbar^2 p^2}{2m_\downarrow} + \Sigma_e(\omega, p)$. This energy is purely real for a slow impurity, in which case the polaron is large and continuum, and the effective mass approximation can be used in this case, i.e., $E = \frac{\hbar^2 p^2}{2m^*} + E_0$ where $E_0 \approx -\frac{g^2}{2m_{e-h}\omega_{e-h}^2} - N_{ph} \frac{\varepsilon_{e-ph}}{\Omega_{ph}^0(q')} < 0$ is the impurity momentum-independent energy of the polaron. The large polaron (compared to the lattice constant) has a small value of hopping and thus with a positive and large binding energy (corresponds to a negative and large polaron energy[73]). The distortion as well as the ions would also slow the large polaron down.

6 polaron-polaron interaction

As we state above, the electron-phonon coupling matrix element $|g_{p+q',p}|^2$, which describes the phonon-induced electron transitions (interband or intraband), depends on both the impurity momentum and phonon momentum in the nonlinear case for q' extended to the K -point (e.g., $q' = 0.665\frac{2\pi}{a}$ for graphene[42]), just like the polaron-polaron interaction vertex as we mention below[72, 69], but it depends only on the phonon momentum q' in the linear case which with adiabatic motion of the impurity. The absorption and emission of phonons which leads to incoherence, and also possible to gives rise to the polaron-polaron interaction, for two impurities with opposite spins, e.g., in the light-enhanced case[77].

The phonon-related polaron-polaron interaction has two kinds. One of them is the phonon-mediated density-density (direct) interaction, which is related to the dielectric function $\epsilon(q', \nu)$ in the method of GW-random phase approximation

(RPA) (or equivalently, the spectral function $A(q')$ in plasmon-pole approximation (PPA)), and we can write the self-energy of such bipolaron as

$$\begin{aligned} \Sigma(p, \omega) = & \int \frac{d\nu}{2\pi} \int \frac{d^2k}{(2\pi)^2} G_0(p-k, \omega-\nu) V_{p-p}(q') + \\ & \int \frac{d\nu}{2\pi} \int \frac{d^2k}{(2\pi)^2} G_0(p-k, \omega-\nu) V_{p-p}(q') [\epsilon^{-1}(q', \nu) - 1], \end{aligned} \quad (35)$$

where the first term is the Hartree-Fock part while the second term is the correlation part. Here $V_{p-p}(q')$ is the polaron-polaron interaction strength, and $\epsilon(q', \nu) = 1 - 2V_{p-p}(q') \sum_p \frac{N_F(p+q') - N_F(p)}{\nu + i\eta + \epsilon_{p+q'} - \epsilon_p}$. In Landau Fermi-liquid theory, the density-density interaction between polarons must be repulsive[1], and the Coulomb interaction is certainly screened. This kind of polaron-polaron interaction is dominate for the 2D system on a polar substrate, and then the effective mass of polaron becomes dependent on both the electron-phonon coupling constant and the phonon occupation factor [102, 103]. In the presence of effective dielectric function, the residue Z also related to the energy loss function as $Z^{-1} = 1 - \pi[-\text{Im}\epsilon^{-1}(q', \nu)]^{-1}$.

The second type of the phonon-related polaron-polaron interaction is the pair-hopping type. We found the interaction vertex of this type of polaron-polaron interaction is similar to the pair propagator as we mention above, which is related to the propagation of a pair of coupled impurity-majority, but for here is happen between a pair of impurity with opposite spins, like the singlet. In this case, the polaron-polaron propagator, for a pair of polarons with separation distance evolve from 1 to n ($n \geq 1$), can be obtained by the Dyson function as $G^{1,n} = G_0^{1,n} + g \sum_{n'} G_0^{n',n} \sum_i \frac{e^{ik(r_i + \frac{n'_i}{2})(r_i + \frac{g}{2})}}{\sqrt{N}} \langle 0 | G(\omega) c_i c_{i+1} c_{i+n'}^\dagger c_{i+n''}^\dagger b_{i+n'-n''}^\dagger | 0 \rangle$, where $G(\omega) = \frac{1}{\omega + i\eta - H_{p-p}}$ is the Green's function of the bipolaron with the Hamiltonian $H_{p-p} = \sum_p \epsilon_p c_p^\dagger c_p + (\Sigma_e + \Pi_e) \sum_p c_p^\dagger c_p + (2(\Sigma_e + \Pi_e) + V_{p-p}) \sum_{pp'Q} c_{p'+Q}^\dagger c_{p-Q}^\dagger c_p c_{p'}$ in momentum space. The unperturbed state $|0\rangle$ could be treated as the vacuum state at zero-temperature limit. Note that here p is no more the momentum of bare impurity but of the polarons. The Green's function here vanishes in the large distance limit $n \rightarrow \infty$ where ω outside the polaron-polaron continuum (unbound) region[78], and equation of motion[79, 80, 78] of this Green's function at ground state (for Brillouin zone boundary) can be obtained as $(\omega + i\eta - [4(\Sigma_e + \Pi_e) + V_{p-p}])G_{1,n} = \delta_{n,1}$. Note that within the Hamiltonian H_{p-p} the interaction vertex $V_{p-p}(p, p', Q)$ (Q is the exchange momentum) takes an important role in the case of translational invariant which guarantees that the total momentum of the bipolaron is a good quantum number. Thus this expression, which described the pair-hopping process, is valid as long as $\frac{\epsilon_{e-ph}}{3t\Omega_{ph}^0} < 1$ since the strong electron-phonon coupling will breaks the translational invariance. Base on Peierls coupling, the avoided crossing in the band structure happen for both the single polaron and the bipolaron when the electron-phonon interaction strength turns up and reaches $\frac{\epsilon_{e-ph}}{3t\Omega_{ph}^0} > 0.5$ [72, 69, 79, 80], which means that the nonadiabaticity appears, and this is more easy to found in the case of large phonon energy. This avoided crossing phenomenon (similar to the band inversion of the topological materials) is very important because it reveals the topological properties of the polaron band structure, and we can see that the polaron indeed shares the topological phase with some of the topological insulator or superconductor [83, 84, 85] no matter it's been formed in the solid state or the ultracold gases[82]. The avoided crossing band structure corresponds to the nonadiabatic (or nonlinear) case where the lowest energy of fermionic excitation does not located at $p = 0$, and it's possible to appears for both the fermi polaron and boson polaron. Besides, due to the strong (interatomic) interaction in this case, the superfluid can emerges within the cloud, and thus the impurity can moves without lossing energy and also without excites other particles. The superfluid in such strong-coupling regime is usually topological trivial and with a chemical potential $\mu < 0$ [113]. That's why the could forms the superfluid can formed within the hard-sphere bosons (with interaction effect) while the free bosons can not. In such a coherent state, the dissipation of the bath is also fastest[32].

7 Conclusion

We construct a model where the composite polaron formed in the surface of a 2D Dirac honeycomb lattice. The impurity is firstly dressed by a cloud of electron-hole pairs (with unequal momenta), and then excited by the phonons. The phonons can be viewed in a coherence state while the existence of electron-phonon coupling for small band gap (absorption and emission of phonons by the impurity) induces the incoherence. In the presence of electron-phonon coupling, it is possible for impurity to has a quadratic dispersion or linear dispersion (due to the effect of Dirac cone which can be treated as a perturbation origin from the relativistic particles). Note that we focus on the weak coupling regime throughout the paper, no matter for the interaction between impurity and the electron-hole pair or that between the impurity and phonons. For electron-phonon coupling, both the adiabatic and nonadiabatic cases are studied (we focus on acoustic phonon). Specially, the avoided crossing of band structure appears for both the single polaron and bipolaron (the pair-hopping one) in nonadiabatic regime, where the perturbation theory becomes more accurate than Migdal-Eliashberg theory. The avoided crossing for bipolaron can be found in the strong-coupling antiadiabatic limit, where the resonance vanishes and the impurity is surrounded by the virtual phonon emission and absorption. For the pair-hopping type bipolaron, which is directly pairing in the real space unlike the density-density type, it remains the coherence property with nonadiabatic motion (for $\frac{\epsilon_{e-ph}}{3t\Omega_{ph}^0} > 0.5$) and it is possible to forms the superfluid at low temperature. This type of bipolaron appears when the next-nearest-neighbor hopping is forbidden by the hard-core

statistics[80, 79] (for spinless Fermions). The method of RPA together with the Ward identity are used in calculating the electron self-energy induced by electron-phonon coupling and the dielectric function which describes the density-density correlation (also the electronic susceptibility) between the polarons (in momentum space). The RPA here is applicable since the phonon momentum q' is small and the electron-phonon coupling is weak in this paper[107].

The dimensionless electron-phonon coupling in GW calculation[110] is slightly different from that in the Peierls (Su-Schrieffer-Heeger) model[72]. The most direct evidence is that the electron-phonon coupling matrix element is independent of the electron momentum p in the former one as applied in Refs.[102, 130], while the p -dependence may emerge for the later one after the Fourier transform of interaction vertex.

Through the density plot of spectral function, we found that the polaronic effect induced modes are damped in the regions of $p - \omega$ space where the imaginary part of self-energy is large. We also found that, for small q' , the effect electron-phonon coupling leads to a linear dispersion in the large-impurity momentum (stable) region (see Fig.3). In the absence of umklapp scattering, this damping dynamics can be well described by the Landau-Fermi liquid theory (for free impurity). This inspires us that, for topological insulator systems, the topologically protected umklapp-free plasmon-polaron mode[98, 107] can emerge and then leads to the band dispersion which is gapless in the middle point of BZ edge—the M point. We can certainly know that such situation corresponds to the antiadiabatic limit which with strong (short-ranged) interaction in the K -point, and can also be observed in the optical honeycomb lattice in the presence of strong interatomic interaction[46]. Furthermore, GW calculation (with dynamically screened Coulomb potential) shows that the band gap in M -point varies with the doping level: when the doping level is made away from zero through the gate voltage (no matter n -type or p -type), accompanied by the increasing short-range (Hubbard-type) electron-electron interaction and decreasing deformation potential[110] (due to the competitive effect between electron-phonon coupling and electron-electron Coulomb repulsion), the gap in M -point decreases. In the other hand, the above mentioned umklapp-free mode provides another way to realize such nonadiabatic dynamics, even when the fermi wave vector is much smaller than phonon one \mathbf{q}' . It relies on the low energy helical character of the topological state, that is, within the first Brillouin zone, for strong enough electron-phonon coupling with $p \ll q'$, we have $\mathbf{p} + \mathbf{q}' \approx \mathbf{q}'$, and the overlap factor $\langle f_{\mathbf{q}'-\mathbf{G}} | f_{\mathbf{q}'} \rangle \rightarrow 0$. This is indeed a nonadiabatic limit since $E_M \ll \Omega_{ph}^0(q') = \beta q'$ where E_M is the absolute value of energy of the lowest conduction band at M -point (note that here $\Omega_{ph}^0(q')$ of the α -mode[107, 102] keeps increasing linearly even when it passes the M -point or K -point[107] which is completely different to the normal monoatomic 2D honeycomb lattices[24]). Also, $p \ll q'$ shows that the impurity moves slowly and the phonons can respond instantaneously to it[102]. The nonadiabaticity can also be seen from the band structure of the helical edge states[111].

In weak coupling regime, both the effective masses induced by the electron-phonon interaction and the interaction between impurity and the electron-hole pair are studied through the approximated and exact expressions. We found that in stable region ($p > 1$), the effective masses increase as q^a with $a > 1$. For impurity with smaller electron energy, the induced effective mass is larger. We also found that, the effective mass derived from approximated expression is larger than that derived from exact expression. The reason for this phenomenon is related to the impurity dispersion (although may be variable in the polaronic dynamics) as explained in the main text.

The polaronic effect investigated here is meaningful to the study of pairing mechanism as well as the phonon-mediated high-temperature superconductivity. For example, the twisted bilayer graphene near the magic angle could induce the superconducting instability[108, 130] with the attractive electron-acoustic phonon interaction which even overcomes the Coulomb repulsion through the retardation effect [130, 109]. The phonon velocity is been estimated as $s = 0.02v_F$ in Ref.[130], and the electron-acoustic phonon coupling will flatten the pristine electron dispersion, and thus lowers the group velocity of electron (narrower bandwidth due to the incoherence). We can also infer that the nonadiabaticity is increased since the strong electron-phonon coupling changes the cone-like dispersion into the avoided crossing-like dispersion[130] and lengthen the relaxation time of impurity-momentum p . In the other hand, due to the lowered slope of bands near Dirac cone, the gap in M point should be reduced, which is also consistent with our above conclusions. It is recently found that at a tilt Weyl semimetal in the presence of electric field and magnetic field, the motion of occupied state along the axis connecting to Weyl nodes with opposite chirality can excite the electron-hole pairs in the momentum space[114] which can be viewed as a chiral anomaly. In the mean time, the deformation-induced vibration, although with the sound velocity much slower than the fermi velocity, can excite the fermi quasiparticle[114]. Then, in the presence of multi-phonon (classical), the polaronic effect as well as the interesting modes mentioned in this paper would be produced in such model.

8 Appendix.A: Peierls model in real space representation

We rewrite the local phonon and the e-ph coupling terms in Eq.(7) in space representation as,

$$\mathcal{H} = H_{ph} + H_{e-ph} = \omega \sum_i b_i^\dagger b_i + g\omega \sum_{ij} (c_i^\dagger c_j + c_j^\dagger c_i)(b_i^\dagger + b_i - b_j^\dagger - b_j). \quad (36)$$

Consider the Peierls phonons quasiclassically as the harmonic oscillators, like the hydrogen bond vibration[145, 146] whose electron trapping effect can be observed by far-infrared spectrum,

$$H_{ph} = \sum_i \left(\frac{q_i^2}{2m_{ph}} + \frac{1}{2} m_{ph} \omega_0^2 x_i^2 \right) = \omega_p \sum_i (\mathcal{P}_i^2 + \mathcal{X}_i^2), \quad (37)$$

where we define

$$\begin{aligned} \mathcal{P}_i &= (b_i^\dagger + b_i - X_i) \cos(\omega_p t), \\ \mathcal{X}_i &= (b_i^\dagger + b_i - X_i) \sin(\omega_p t), \\ X_i &= b_i^\dagger + b_i - \sqrt{b_i b_i^\dagger}. \end{aligned} \quad (38)$$

In terms of a canonical momentum-related function $f(\hat{\mathcal{P}}_i) := b_i^\dagger + b_i - X_i = \sqrt{b_i^\dagger b_i}$ and the canonical coordinate $\hat{\mathcal{X}}_i := \omega_p t$, we can apply the Poisson bracket, $\frac{\partial \mathcal{P}_i}{\partial \mathcal{P}_i} \frac{\partial \mathcal{X}_i}{\partial \hat{\mathcal{X}}_i} - \frac{\partial \mathcal{P}_i}{\partial \hat{\mathcal{X}}_i} \frac{\partial \mathcal{X}_i}{\partial \mathcal{P}_i} = 1$, and obtain $f(\hat{\mathcal{P}}_i) = \sqrt{2\hat{\mathcal{P}}_i}$.

In terms of the Holstein phonon-assisted electron relaxation, the current in time domain reads[142]

$$J(t) = -i g_p \omega_p \sum_{ij} (c_i^\dagger c_j - c_j^\dagger c_i) ([b_i^\dagger + b_i](t) - [b_j^\dagger + b_j](t)), \quad (39)$$

which can be cast into the following simple form

$$J(t) = \sum_{ij} J_{ij}(t) c_i^\dagger c_j, \quad (40)$$

with J_{ij} a Peierls phonons-related strength constant which could be Gaussian distributed.

Most importantly, the effect of classical time evolution on the current-current correlation can be estimated by the following equality

$$\begin{aligned} \mathcal{C}_{JJ}(t) &= \frac{\text{Tr}[J(t)J(0)e^{-\beta H}]}{\text{Tr}e^{-\beta H}} \\ &= \sum_{\mathcal{P}, \mathcal{X}} F(\mathcal{P}, \mathcal{X}) \frac{\text{Tr}[e^{i \int_0^t d\tau H(\tau)} J(t) e^{-i \int_0^t d\tau H(\tau)} J(0) e^{-\beta H}]}{\text{Tr}e^{-\beta H}}, \end{aligned} \quad (41)$$

where $F(\mathcal{P}, \mathcal{X})$ is the phase-space distribution of the classical Peierls variables.

In low-carrier-density limit, the dc conductivity in the presence of weak-binding-energy-supported polaron provides the well-defined mobility (or ideal conductivity; due to the absence of ergodicity) $\mu_m = \sigma_{dc}/n$. While at high electron concentration, the long-range charge order or the superconductivity is possible to form. When the long-range Coulomb effect enhance the mobility, the Peierls polaron becomes unstable, which is in agree with the semilocal generalized gradient approximation (GGA) as well as the experimentally observed higher conductivity in anatase compares to rutile[143]. As higher mobility will delocalize the charge density and suppress the formation of polaron. The method of DFT+U (with the Hubbard interaction estimated from RPA) as well as the range-hybrid approaches (which gives rise to piecewise linear), aiming at the localization correction, but sometimes they still underestimate the band gap and Coulomb screening, i.e., overestimate the mobility, and thus leads to an unstable Peierls-type polaron. Similar reason results in the different results by IR spectroscopy and STM or optical absorption[143], where the IR spectroscopy usually closes to the result predicted by large mobility as well as the Holstein model. Thus the comparison between IR spectral and the optical absorption one can help to estimate the competition between localization (small Holstein polaron) and delocalization (large Peierls polaron) effect. Compares to WTe₂ which has a good (low-resistance) Ohmic contact as can be verified by its nearly linear current-voltage (I-V) curve. In contrast, the WSe₂ usually has a higher resistance for Ohmic contact due to the existence of Schottky barrier. Since WSe₂ is a semiconductor with high mobility, and it is more easy to realizing the n-type doping (using potassium or lithium), a low work function contact metal is often used as the electrode[144]. Thus our study on the polaronic dynamic concerning the surface charge trapping and its effect to the system mobility is also helpful in solve the problem of high-resistance Ohmic contact in both the chemically or electrostatically ways.

9 Appendix.B: ZA phonon mode with higher order dispersion: $\Omega_{ph}^0(q') = q'^\alpha (\alpha > 2)$

From the Fig.6, we can see that, for $p < 2.5$, the effective mass Δm^* diverges dramatically at certain momenta p and impurity frequencies ω . Such divergence of effective mass origins from the instability of the fermi polaron (as a

metastable excitation which is the origin of the small imaginary part in the right-hand-side of Eq.(27)), and it has also been found in the strong coupling region of Bose polaron in a condensate [86, 87, 88]. We note that the effective masses obtained here have the negative part, furthermore, the region where $m_0 + \Delta m^* < 0$ can be viewed as a signal of the emergence of avoided crossing dispersion (nonadiabatic), which implies that the minimum of fermi polaron dispersion is not at $p = 0$ [90] (because in effective mass approximation the negative kinetic term leads to larger momentum-independent polaron energy than the total one) and thus also signals the instability[89]. We will see in the following that this is in contrast to the effective mass induced by electron-phonon coupling, which is completely positive over the whole momentum range (for small finite β). We also found that, for $p \geq 2.5$, the effective mass is always positive. In Fig.7, we plot the results of the induced effective masses within such a fermi polaron through the exact expression (upper panels) approximated expression (lower panels) of the effective mass ($\Delta m^* = -[\frac{\partial^2 E(p)}{\partial p^2}]^{-1} = [\frac{\partial^2 |E(p)|}{\partial p^2}]^{-1}$ and $\Delta m^* = p/\frac{\partial E(p)}{\partial p}$, respectively). We can see that in large impurity momentum ($p > 1.5$) the effective mass increase powerly with p and decrease with ω .

In Fig.8-9, we show both the exact result $\Delta m^* = -[\frac{\partial^2 E(p)}{\partial p^2}]^{-1}$ and the approximated result of the effective mass Δm^* induced by the electron-phonon coupling, for free impurity (quadratic dispersion) and the one near Dirac cone (the Dirac cone could be viewed as a defect or perturbation but we do not consider its topological properties here, i.e., without the spin/pseudospin-momentum coupling), respectively. We can see from the figures that the effective mass obtained through the approximated expression is larger than the exact one. From the expressions of the induced effective mass, we can know that the approximated effective mass only takes the second-order dispersion of momentum p into account, which makes it more accurate for the impurity with quadratic dispersion. That is why the approximated results (the full-line) in Fig.9 is farther away from the exact results (the dashed-line) than Fig.8. Here for the Dirac-type (initial) impurity electron, we suppose the linear dispersion $\varepsilon_p = \alpha p$ where we set $\alpha \approx 30\beta$ (for LA) according to the first-principle calculations[24, 81], i.e., the group velocity of the Dirac Fermi quasiparticle $\partial E(p)/\partial p = \alpha$ is much larger than the sound velocity. That allows the quasiparticle decaying to happen through the emission of phonons, and also gives rise to the finite spectral width base on the BCS-type particle-quasiparticle (or quasiparticle-quasiparticle) interaction (like the third term of Eq.(20) with a finite exchange momentum q). For attractive polaron ($a_{\psi\phi} < 0$), the broadening of the spectral function of polaron vanishes at the minimum of particle-branch or the maximum of hole-branch when the gap between these two branches is zero, because there has no enough phase space for quasiparticles to decay. Note that the polaron branches are parabolic here, so that the group velocity α could becomes smaller than the sound velocity $s\beta$ (when consider the interaction between impurity and the phonon (gapless boson quasiparticle)) in the level closest to the chemical potential (e.g., μ_{\uparrow}). This phenomenon is also been verified by our previous work[5] and other Refs.[82, 19]. Also, we can clearly find that the induced effective mass for impurity which is initially a Dirac-like electron (Fig.9) is much larger than the one which is initially a conventional electron (Fig.8). That is reasonable because it requires stronger interaction strength to excites a initially linear Dirac electron to a quadratic electron (e.g., enters into the surface 2D electron gas), and then through the expression of effective mass given above we can easily know that the impurity has larger effective mass.

Here for effective masses induced by both the impurity-electron-hole pair interaction and the electron-phonon coupling, we have $Z \rightarrow 1$ when $\Delta m^* \rightarrow 0$, i.e., the noninteracting particles is totally dominating. In this case, for fermi polaron with $\omega \neq 0$ (see Fig.5(a)), in the region where the imaginary part of self-energy (impurity damping rate) acts as $\sim \omega^a$ ($a > 1$), the residue Z tends to a small but nonzero value in the limit of vanishing fermi energy, which means that the fermi-liquid theory as well as the perturbation theory are still applicable in this scenario[91, 92] (while for bose polaron, an additional requirement is the nonadiabatic limit). We note that the consideration of multiple particle-hole excitations become important in the strong coupling regime where $Z \rightarrow 0$. For impurity with quadratic dispersion, the residue will remains finite even in the zero-energy limit, and it has smaller value in nonadiabatic case compared to the adiabatic case due to the coherent effect.

In Fig.10, we show the quasiparticle residue, self-energy of the composite polaron which containing the effects of both the fermi polaron and electron-phonon coupling. According to the self-energy computed above (Fig.2 and Fig.5), we can see that the composite polaron is stable (well-defined) only when the momentum larger or comparable with 1, above where the imaginary part of the self-energy tends to zero. This means that it is only meaningful to observe the related physical quantities in the region $p \geq 1$ (the exact value of momentum varies with impurity frequency), while in the low momentum region, the nonadiabatic effect may induce the instabilities. From Fig.10, we can see that the quasiparticle residue is very close to 1 ($Z \gtrsim 0.9$) for $p \geq 1$, and the self-energy is also always negative in this momentum region, which implies that the composite polaron still has an attractive overall effect. As we stated above, here the self-energy of composite polaron is obtained by the relation $\text{Re}\Sigma(E(p), p) = \text{Re}\Sigma_e(\omega, p) + \text{Re}\Pi_e(p)$. The large residue Z is also agrees with the restriction of weak interaction throughout this paper.

References

- [1] Scazza F, Valtolina G, Massignan P, et al. Repulsive Fermi polarons in a resonant mixture of ultracold Li 6 atoms[J]. Physical review letters, 2017, 118(8): 083602.
- [2] Li W, Sarma S D. Variational study of polarons in Bose-Einstein condensates[J]. Physical Review A, 2014, 90(1): 013618.
- [3] Fratini E, Pieri P. Mass imbalance effect in resonant Bose-Fermi mixtures[J]. Physical Review A, 2012, 85(6): 063618.
- [4] Sidler M, Back P, Cotlet O, et al. Fermi polaron-polaritons in charge-tunable atomically thin semiconductors[J]. Nature Physics, 2017, 13(3): 255.
- [5] Wu C H. Attractive fermi polaron in a semi-Dirac system within ladder approximation[J]. arXiv preprint arXiv:1901.07881, 2019.
- [6] Wu C H. Attractive polaron in a Dirac system within ladder approximation[J]. arXiv preprint arXiv:1812.04833, 2018.
- [7] Qin F, Cui X, Yi W. Polaron in a $p + ip$ Fermi topological superfluid[J]. arXiv preprint arXiv:1901.02766, 2019.

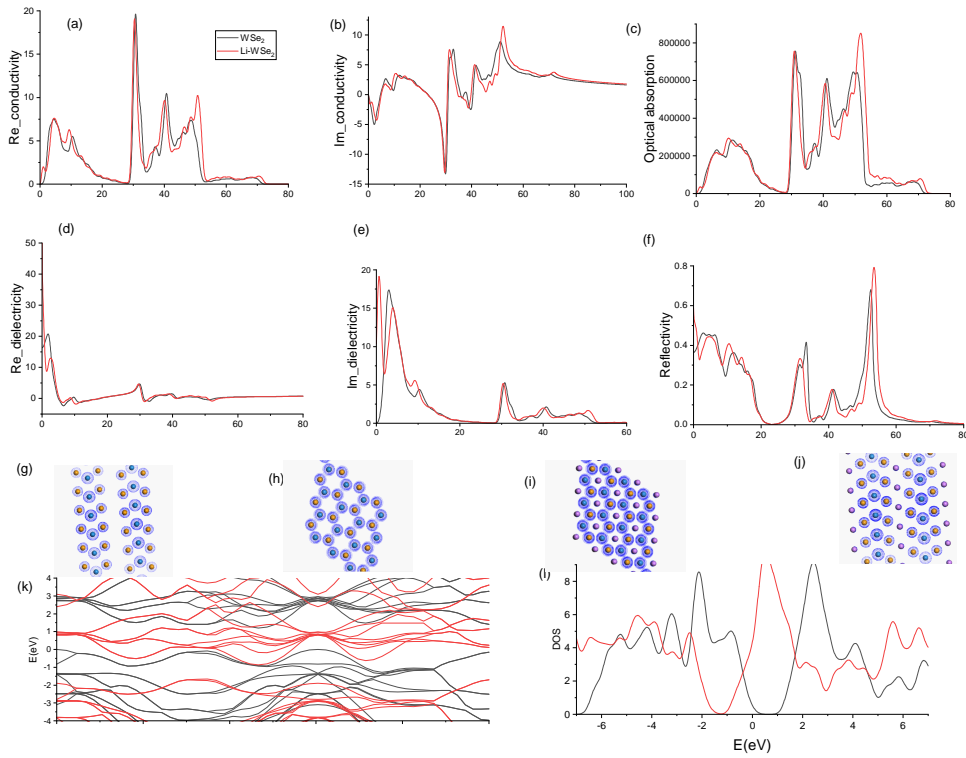


Figure 1: DFT study for the pristine and Li-doped WSe_2 . In Li-doped WSe_2 as a n-type semiconductor, the Li provided extra electrons and slightly localized the electrons around it, and thus lower the charge mobility as can be seen from the larger charge distance between the sphere of the charge densities. (a)-(f) show the optical conductivity, absorption, dielectricity, reflectivity, where x-axis is the frequency in unit of eV. (g)-(j) show the charge density of WSe_2 before and after Li doping. The optical conductivity and dielectricity also in agree with this statement: The doped WSe_2 has a lower (in average) conductivity and higher dielectricity (in zero frequency limit), higher absorption, higher reflectivity, compares to the pristine one, which indicates its lower mobility and stronger Coulomb screening (which cause the charge localization).

- [8] Caldas H, Mota A L, Farias R L S, et al. Superfluidity in two-dimensional imbalanced Fermi gases[J]. *Journal of Statistical Mechanics: Theory and Experiment*, 2012, 2012(10): P10019.
- [9] Wang D W, Lukin M D, Demler E. Engineering superfluidity in Bose-Fermi mixtures of ultracold atoms[J]. *Physical Review A*, 2005, 72(5): 051604.
- [10] Kinnunen J J, Wu Z, Bruun G M. Induced p-wave pairing in Bose-Fermi mixtures[J]. *Physical review letters*, 2018, 121(25): 253402.
- [11] Fukuhara T, Kantian A, Endres M, et al. Quantum dynamics of a mobile spin impurity[J]. *Nature Physics*, 2013, 9(4): 235.
- [12] Koschorreck M, Pertot D, Vogt E, et al. Attractive and repulsive Fermi polarons in two dimensions[J]. *Nature*, 2012, 485(7400): 619.
- [13] Kasprzak J, Richard M, Kundermann S, et al. Bose-Einstein condensation of exciton polaritons[J]. *Nature*, 2006, 443(7110): 409.
- [14] Camacho-Guardian A, Goldman N, Massignan P, et al. Dropping an impurity into a Chern insulator: a polaron view on topological matter[J]. *Physical Review B*, 2019, 99(8): 081105.
- [15] Polini M, Asgari R, Borghi G, et al. Plasmons and the spectral function of graphene[J]. *Physical Review B*, 2008, 77(8): 081411.
- [16] Wang Z, Zhao J, Frank B, et al. Plasmon-polaron coupling in conjugated polymer on infrared nanoantennas[J]. *Nano letters*, 2015, 15(8): 5382-5387.
- [17] Blume D. Efimov physics and the three-body parameter for shallow van der Waals potentials[J]. *Few-Body Systems*, 2015, 56(11-12): 859-867.
- [18] Wang Y, Julienne P S. Universal van der Waals physics for three cold atoms near Feshbach resonances[J]. *Nature Physics*, 2014, 10(10): 768.
- [19] Rath S P, Schmidt R. Field-theoretical study of the Bose polaron[J]. *Physical Review A*, 2013, 88(5): 053632.
- [20] Narayanaswamy A, Zheng Y. van der Waals energy and pressure in dissipative media: Fluctuational electrostatics and mode summation[J]. *Physical Review A*, 2013, 88(1): 012502.
- [21] Chen C, Avila J, Wang S, et al. Emergence of Interfacial Polarons from Electron-Phonon Coupling in Graphene/h-BN van der Waals Heterostructures[J]. *Nano letters*, 2018, 18(2): 1082-1087.
- [22] Massignan P. Polarons and dressed molecules near narrow Feshbach resonances[J]. *EPL (Europhysics Letters)*, 2012, 98(1): 10012.
- [23] Bruun G M, Jackson A D, Kolomeitsev E E. Multichannel scattering and Feshbach resonances: Effective theory, phenomenology, and many-body effects[J]. *Physical Review A*, 2005, 71(5): 052713.
- [24] Ge X J, Yao K L, Lü J T. Comparative study of phonon spectrum and thermal expansion of graphene, silicene, germanene, and blue phosphorene[J]. *Physical Review B*, 2016, 94(16): 165433.
- [25] Combescot R, Giraud S. Normal state of highly polarized Fermi gases: full many-body treatment[J]. *Physical review letters*, 2008, 101(5): 050404.
- [26] Levine M, Tjon J, Wright J. Nonsingular Bethe-Salpeter Equation[J]. *Physical Review Letters*, 1966, 16(21): 962.
- [27] Karmanov V A, Carbonell J. Solving Bethe-Salpeter equation in Minkowski space[J]. *The European Physical Journal A-Hadrons and Nuclei*, 2006, 27(1): 1-9.
- [28] Camacho-Guardian A, Ardila L A P, Pohl T, et al. Bipolarons in a Bose-Einstein condensate[J]. *Physical review letters*, 2018, 121(1): 013401.
- [29] Diestler D J, Zewail A H. Vibronic dephasing of anharmonic molecules. I. Theory and its application to the separability of intra-and intermolecular processes[J]. *The Journal of Chemical Physics*, 1979, 71(7): 3103-3112.
- [30] Andrews M R, Kurn D M, Miesner H J, et al. Propagation of sound in a Bose-Einstein condensate[J]. *Physical review letters*, 1997, 79(4): 553.
- [31] Nielsen K K, Ardila L A P, Bruun G M, et al. Critical slowdown of non-equilibrium polaron dynamics[J]. *New Journal of Physics*, 2019.
- [32] Visuri A M, Kinnunen J J, Baarsma J E, et al. Decoherence of an impurity in a one-dimensional fermionic bath with mass imbalance[J]. *Physical Review A*, 2016, 94(1): 013619.
- [33] Hadzibabic Z, Krüger P, Cheneau M, et al. Berezinskii-Kosterlitz-Thouless crossover in a trapped atomic gas[J]. *Nature*, 2006, 441(7097): 1118.
- [34] Merkl M, Jacob A, Zimmer F E, et al. Chiral confinement in quasirelativistic Bose-Einstein condensates[J]. *Physical review letters*, 2010, 104(7): 073603.
- [35] Haddad L H, Carr L D. The nonlinear Dirac equation in Bose-Einstein condensates: Foundation and symmetries[J]. *Physica D: Nonlinear Phenomena*, 2009, 238(15): 1413-1421.
- [36] Kim N Y, Kusudo K, Löffler A, et al. Exciton-polariton condensates near the Dirac point in a triangular lattice[J]. *New Journal of Physics*, 2013, 15(3): 035032.
- [37] Mahan G D. *Many-particle physics*[M]. Springer Science & Business Media, 2013.
- [38] Li X, Mullen J T, Jin Z, et al. Intrinsic electrical transport properties of monolayer silicene and MoS₂ from first principles[J]. *Physical Review B*, 2013, 87(11): 115418.
- [39] Matthes L, Gori P, Pulci O, et al. Universal infrared absorbance of two-dimensional honeycomb group-IV crystals[J]. *Physical Review B*, 2013, 87(3): 035438.
- [40] Borysenko K M, Mullen J T, Barry E A, et al. First-principles analysis of electron-phonon interactions in graphene[J]. *Physical Review B*, 2010, 81(12): 121412.
- [41] Yan J A, Stein R, Schaefer D M, et al. Electron-phonon coupling in two-dimensional silicene and germanene[J]. *Physical Review B*, 2013, 88(12): 121403.
- [42] Yan J A, Ruan W Y, Chou M Y. Electron-phonon interactions for optical-phonon modes in few-layer graphene: First-principles calculations[J]. *Physical Review B*, 2009, 79(11): 115443.
- [43] Alexandrov A S. Breakdown of the Migdal-Eliashberg theory in the strong-coupling adiabatic regime[J]. *EPL (Europhysics Letters)*, 2001, 56(1): 92.
- [44] Gusynin V P, Sharapov S G. Transport of Dirac quasiparticles in graphene: Hall and optical conductivities[J]. *Physical Review B*, 2006, 73(24): 245411.
- [45] Pyatkovskiy P K. Dynamical polarization, screening, and plasmons in gapped graphene[J]. *Journal of Physics: Condensed Matter*, 2008, 21(2): 025506.
- [46] Chen Z, Wu B. Bose-Einstein condensate in a honeycomb optical lattice: Fingerprint of superfluidity at the Dirac point[J]. *Physical review letters*, 2011, 107(6): 065301.
- [47] Liu J, Wu B, Niu Q. Nonlinear evolution of quantum states in the adiabatic regime[J]. *Physical review letters*, 2003, 90(17): 170404.
- [48] Wu B, Niu Q. Nonlinear Landau-Zener tunneling[J]. *Physical Review A*, 2000, 61(2): 023402.
- [49] Liu J, Fu L, Ou B Y, et al. Theory of nonlinear Landau-Zener tunneling[J]. *Physical Review A*, 2002, 66(2): 023404.
- [50] Liu F, Liu C C, Wu K, et al. d+id Chiral Superconductivity in Bilayer Silicene[J]. *Physical review letters*, 2013, 111(6): 066804.
- [51] Yi W, Zhang W. Molecule and polaron in a highly polarized two-dimensional Fermi gas with spin-orbit coupling[J]. *Physical review letters*, 2012, 109(14): 140402.
- [52] Chen J G, Deng T S, Yi W, et al. Polarons and molecules in a Fermi gas with orbital Feshbach resonance[J]. *Physical Review A*, 2016, 94(5): 053627.
- [53] Band Y B, Trippenbach M. Bose-Einstein condensates in time-dependent light potentials: Adiabatic and nonadiabatic behavior of nonlinear wave equations[J]. *Physical Review A*, 2002, 65(5): 053602.
- [54] Berman O L, Lozovik Y E, Gumbs G. Bose-Einstein condensation and superfluidity of magnetoexcitons in bilayer graphene[J]. *Physical Review B*, 2008, 77(15): 155433.
- [55] Min H, Bistrizter R, Su J J, et al. Room-temperature superfluidity in graphene bilayers[J]. *Physical Review B*, 2008, 78(12): 121401.
- [56] Blakie P B, Clark C W. Wannier states and Bose-Hubbard parameters for 2D optical lattices[J]. *Journal of Physics B: Atomic, Molecular and Optical Physics*, 2004, 37(7): 1391.
- [57] Wu B, Niu Q. Superfluidity of Bose-Einstein condensate in an optical lattice: Landau-Zener tunnelling and dynamical instability[J]. *New journal of Physics*, 2003, 5(1): 104.
- [58] Wellein G, Röder H, Fehske H. Polarons and bipolarons in strongly interacting electron-phonon systems[J]. *Physical Review B*, 1996, 53(15): 9666.
- [59] Alexandrov A S, Mott N F. Bipolarons[J]. *Reports on Progress in Physics*, 1994, 57(12): 1197.
- [60] Jotzu G, Messer M, Grg F, et al. Creating state-dependent lattices for ultracold fermions by magnetic gradient modulation[J]. *Physical review letters*, 2015, 115(7): 073002.
- [61] Kohstall C, Zaccanti M, Jag M, et al. Metastability and coherence of repulsive polarons in a strongly interacting Fermi mixture[J]. *Nature*, 2012, 485(7400): 615.
- [62] Carneiro L M, Cushing S K, Liu C, et al. Excitation-wavelength-dependent small polaron trapping of photoexcited carriers in α -Fe₂O₃[J]. *Nature materials*, 2017, 16(8): 819.
- [63] Vlietinck J, Ryckebusch J, Van Houcke K. Diagrammatic Monte Carlo study of the Fermi polaron in two dimensions[J]. *Physical Review B*, 2014, 89(8): 085119.
- [64] Panochko G, Pastukhov V, Vakarchuk I. Behavior of the impurity atom in a weakly-interacting Bose gas[J]. *arXiv preprint arXiv:1703.10390*, 2017.

- [65] Giustino F, Cohen M L, Louie S G. Electron-phonon interaction using Wannier functions[J]. *Physical Review B*, 2007, 76(16): 165108.
- [66] Perebeinos V, Tersoff J, Avouris P. Electron-phonon interaction and transport in semiconducting carbon nanotubes[J]. *Physical review letters*, 2005, 94(8): 086802.
- [67] Muntwiler M, Yang Q, Tisdale W A, et al. Coulomb barrier for charge separation at an organic semiconductor interface[J]. *Physical review letters*, 2008, 101(19): 196403.
- [68] Verissimo-Alves M, Capaz R B, Koiller B, et al. Polarons in carbon nanotubes[J]. *Physical review letters*, 2001, 86(15): 3372.
- [69] Sous J, Chakraborty M, Krems R V, et al. Light bipolarons stabilized by Peierls electron-phonon coupling[J]. *Physical review letters*, 2018, 121(24): 247001.
- [70] Allen P B. Neutron spectroscopy of superconductors[J]. *Physical Review B*, 1972, 6(7): 2577.
- [71] Zijlstra E S, Tatarinova L L, Garcia M E. Laser-induced phonon-phonon interactions in bismuth[J]. *Physical Review B*, 2006, 74(22): 220301.
- [72] Marchand D J J, De Filippis G, Cataudella V, et al. Sharp transition for single polarons in the one-dimensional Su-Schrieffer-Heeger model[J]. *Physical review letters*, 2010, 105(26): 266605.
- [73] Piegari E, Cataudella V, Ramaglia V M, et al. Comment on “polarons in carbon nanotubes”[J]. *Physical review letters*, 2002, 89(4): 049701.
- [74] Knupfer M, Pichler T, Golden M S, et al. Size of electron-hole pairs in n-conjugated systems[J]. *Physical review letters*, 1999, 83(7): 1443.
- [75] Combescot R, Recati A, Lobo C, et al. Normal state of highly polarized Fermi gases: simple many-body approaches[J]. *Physical review letters*, 2007, 98(18): 180402.
- [76] Devreese J T, Alexandrov A S. Fröhlich polaron and bipolaron: recent developments[J]. *Reports on Progress in Physics*, 2009, 72(6): 066501.
- [77] Sentef M A. Light-enhanced electron-phonon coupling from nonlinear electron-phonon coupling[J]. *Physical Review B*, 2017, 95(20): 205111.
- [78] Berciu M. Few-particle Green's functions for strongly correlated systems on infinite lattices[J]. *Physical review letters*, 2011, 107(24): 246403.
- [79] Sous J, Berciu M, Krems R V. Bipolarons bound by repulsive phonon-mediated interactions[J]. *Physical Review A*, 2017, 96(6): 063619.
- [80] Sous J, Chakraborty M, Adolphs C P J, et al. Phonon-mediated repulsion, sharp transitions and (quasi) self-trapping in the extended Peierls-Hubbard model[J]. *Scientific reports*, 2017, 7(1): 1169.
- [81] Yao Y, Ye F, Qi X L, et al. Spin-orbit gap of graphene: First-principles calculations[J]. *Physical Review B*, 2007, 75(4): 041401.
- [82] Haussmann R, Punk M, Zwerger W. Spectral functions and rf response of ultracold fermionic atoms[J]. *Physical Review A*, 2009, 80(6): 063612.
- [83] Grusdt F, Yao N Y, Demler E. Topological polarons, quasiparticle invariants and their detection in 1D symmetry-protected phases[J]. *arXiv preprint arXiv:1904.00220*, 2019.
- [84] Qi F, Cao J, Cao J, et al. Topological phase transition based on the attractive Hubbard model[J]. *arXiv preprint arXiv:1904.00171*, 2019.
- [85] Ezawa M. Valley-polarized metals and quantum anomalous Hall effect in silicene[J]. *Physical review letters*, 2012, 109(5): 055502.
- [86] Ardila L A P, Giorgini S. Impurity in a Bose-Einstein condensate: Study of the attractive and repulsive branch using quantum Monte Carlo methods[J]. *Physical Review A*, 2015, 92(3): 033612.
- [87] Ichmoukhamedov T, Tempere J. Feynman path-integral treatment of the Bose polaron beyond the Fröhlich model[J]. *arXiv preprint arXiv:1905.07368*, 2019.
- [88] Van Loon S, Casteels W, Tempere J. Ground-state properties of interacting Bose polarons[J]. *Physical Review A*, 2018, 98(6): 063631.
- [89] Combescot R, Giraud S, Leyronas X. Analytical theory of the dressed bound state in highly polarized Fermi gases[J]. *EPL (Europhysics Letters)*, 2010, 88(6): 60007.
- [90] Parish M M, Levinsen J. Highly polarized Fermi gases in two dimensions[J]. *Physical Review A*, 2013, 87(3): 033616.
- [91] Christensen R S, Levinsen J, Bruun G M. Quasiparticle properties of a mobile impurity in a Bose-Einstein condensate[J]. *Physical review letters*, 2015, 115(16): 160401.
- [92] Wang J R, Liu G Z, Zhang C J. Breakdown of Fermi liquid theory in topological multi-Weyl semimetals[J]. *Physical Review B*, 2018, 98(20): 205113.
- [93] Cinquanta E, Meggiolaro D, Motti S G, et al. Ultrafast THz Probe of Photoinduced Polarons in Lead-Halide Perovskites[J]. *Physical review letters*, 2019, 122(16): 166601.
- [94] Kopnin N B, Sonin E B. BCS superconductivity of Dirac electrons in graphene layers[J]. *Physical review letters*, 2008, 100(24): 246808.
- [95] Punk M, Dumitrescu P T, Zwerger W. Polaron-to-molecule transition in a strongly imbalanced Fermi gas[J]. *Physical Review A*, 2009, 80(5): 053605.
- [96] Wong W P D, Yin J, Chaudhary B, et al. Large Polaron Generation and Dynamics in 3D Metal-Halide Perovskites[J]. *arXiv preprint arXiv:1905.11704*, 2019.
- [97] Dong X Y, Li R Z, Deng J P, et al. Interlayer exciton-polaron effect in transition metal dichalcogenides van der Waals heterostructures[J]. *Journal of Physics and Chemistry of Solids*, 2019.
- [98] Shvonski A, Kong J, Kempa K. Plasmon-polaron of the topological metallic surface states[J]. *Physical Review B*, 2019, 99(12): 125148.
- [99] ZZ Yan, Y Ni, C Robens, MW Zwerlein. Bose polarons near quantum criticality. *arXiv preprint arXiv:1904.02685*
- [100] Burkov A A, Hook M D, Balents L. Topological nodal semimetals[J]. *Physical Review B*, 2011, 84(23): 235126.
- [101] Jafari S A, Baskaran G. Equations-of-motion method for triplet excitation operators in graphene[J]. *Journal of Physics: Condensed Matter*, 2012, 24(9): 095601.
- [102] Zhang S, Wei T, Guan J, et al. Enhanced Superconducting State in FeSe/SrTiO₃ by a Dynamic Interfacial Polaron Mechanism[J]. *Physical review letters*, 2019, 122(6): 066802.
- [103] Wong W P D, Yin J, Chaudhary B, et al. Large Polaron Generation and Dynamics in 3D Metal-Halide Perovskites[J]. *arXiv preprint arXiv:1905.11704*, 2019.
- [104] Vukmirović N, Bruder C, Stojanović V M. Electron-phonon coupling in crystalline organic semiconductors: microscopic evidence for nonpolaronic charge carriers[J]. *Physical review letters*, 2012, 109(12): 126407.
- [105] Attaccalite C, Wirtz L, Lazzeri M, et al. Doped graphene as tunable electron-phonon coupling material[J]. *Nano letters*, 2010, 10(4): 1172-1176.
- [106] Wu F, Hwang E, Sarma S D. Phonon-induced giant linear-in-T resistivity in magic angle twisted bilayer graphene: Ordinary strangeness and exotic superconductivity[J]. *Physical Review B*, 2019, 99(16): 165112.
- [107] Jia X, Zhang S, Sankar R, et al. Anomalous acoustic plasmon mode from topologically protected states[J]. *Physical review letters*, 2017, 119(13): 136805.
- [108] Cao Y, Fatemi V, Fang S, et al. Unconventional superconductivity in magic-angle graphene superlattices[J]. *Nature*, 2018, 556(7699): 43.
- [109] Wellein G, Röder H, Fehske H. Polarons and bipolarons in strongly interacting electron-phonon systems[J]. *Physical Review B*, 1996, 53(15): 9666.
- [110] Attaccalite C, Wirtz L, Lazzeri M, et al. Doped graphene as tunable electron-phonon coupling material[J]. *Nano letters*, 2010, 10(4): 1172-1176.
- [111] Michiardi M, Aguilera I, Bianchi M, et al. Bulk band structure of Bi₂Te₃[J]. *Physical Review B*, 2014, 90(7): 075105.
- [112] Altman E, Auerbach A. Oscillating superfluidity of bosons in optical lattices[J]. *Physical review letters*, 2002, 89(25): 250404.
- [113] Qin F, Cui X, Yi W. Polaron in a p+ip Fermi topological superfluid[J]. *Physical Review A*, 2019, 99(3): 033613.
- [114] Zubkov M A, Lewkowicz M. The type II Weyl semimetals at low temperatures: Chiral anomaly, elastic deformations, zero sound[J]. *Annals of Physics*, 2018, 399: 26-52.
- [115] Shubnyi V O, Skrypnik Y V, Sharapov S G, et al. Effect of resonant impurity scattering of carriers on the Drude-peak broadening in uniaxially strained graphene[J]. *Physical Review B*, 2019, 99(23): 235421.
- [116] Rosch A, Kopp T. Heavy particle in a d-dimensional fermionic bath: A strong coupling approach[J]. *Physical review letters*, 1995, 75(10): 1988.
- [117] Kantian A, Schollwöck U, Giamarchi T. Competing regimes of motion of 1D mobile impurities[J]. *Physical review letters*, 2014, 113(7): 070601.
- [118] Meden V, Schmitteckert P, Shannon N. Orthogonality catastrophe in a one-dimensional system of correlated electrons[J]. *Physical Review B*, 1998, 57(15): 8878.
- [119] Wu C H. Electronic properties of the Dirac and Weyl systems with first-and higher-order dispersion in non-Fermi-liquid picture[J]. *arXiv preprint arXiv:1811.08809*, 2018.
- [120] Bhandari S, Cheung M S, Geva E, et al. Fundamental gaps of condensed-phase organic semiconductors from single-molecule calculations using polarization-consistent optimally tuned screened range-separated hybrid functionals[J]. *Journal of Chemical Theory and Computation*, 2018, 14(12): 6287-6294.
- [121] Ong Z Y, Pop E. Effect of substrate modes on thermal transport in supported graphene[J]. *Physical Review B*, 2011, 84(7): 075471.
- [122] Giustino F. Electron-phonon interactions from first principles[J]. *Reviews of Modern Physics*, 2017, 89(1): 015003.
- [123] Hwang E H, Sarma S D. Acoustic phonon scattering limited carrier mobility in two-dimensional extrinsic graphene[J]. *Physical Review B*, 2008, 77(11): 115449.

- [124] Bistritzer R, MacDonald A H. Electronic cooling in graphene[J]. *Physical Review Letters*, 2009, 102(20): 206410.
- [125] Schmidt R, Enss T. Excitation spectra and rf response near the polaron-to-molecule transition from the functional renormalization group[J]. *Physical Review A*, 2011, 83(6): 063620.
- [126] Kim S, Woo S, Min H. Vertex corrections to the dc conductivity in anisotropic multiband systems[J]. *Physical Review B*, 2019, 99(16): 165107.
- [127] Pyatkovskiy P K. Dynamical polarization, screening, and plasmons in gapped graphene[J]. *Journal of Physics: Condensed Matter*, 2008, 21(2): 025506.
- [128] Hwang E H, Throckmorton R E, Sarma S D. Plasmon-pole approximation for many-body effects in extrinsic graphene[J]. *Physical Review B*, 2018, 98(19): 195140.
- [129] Tsuchiya S, Watanabe R, Ohashi Y. Single-particle properties and pseudogap effects in the BCS-BEC crossover regime of an ultracold Fermi gas above T_c [J]. *Physical Review A*, 2009, 80(3): 033613.
- [130] Wu F, Qu F, MacDonald A H. Exciton band structure of monolayer MoS₂[J]. *Physical Review B*, 2015, 91(7): 075310.
- [131] Rana F, George P A, Strait J H, et al. Carrier recombination and generation rates for intravalley and intervalley phonon scattering in graphene[J]. *Physical Review B*, 2009, 79(11): 115447.
- [132] Borysenko K M, Mullen J T, Barry E A, et al. First-principles analysis of electron-phonon interactions in graphene[J]. *Physical Review B*, 2010, 81(12): 121412.
- [133] Alexandrov A, Capellmann H. Phonons in a strongly coupled electron-phonon system[J]. *Physical Review B*, 1991, 43(3): 2042.
- [134] Sio W H, Verdi C, Ponc e S, et al. Ab initio theory of polarons: Formalism and applications[J]. *Physical Review B*, 2019, 99(23): 235139.
- [135] Nocera A, Sous J, Feiguin A E, et al. Bipolaron liquids at strong Peierls electron-phonon couplings[J]. *Physical Review B*, 2021, 104(20): L201109.
- [136] Parish M M. Polaron-molecule transitions in a two-dimensional Fermi gas[J]. *Physical Review A*, 2011, 83(5): 051603.
- [137] Jiang Y, Fan Y, Li S, et al. Photocatalytic Methane Conversion: Insight into the Mechanism of C (sp³)-H Bond Activation[J]. *CCS Chemistry*, 2023, 5(1): 30-54.
- [138] Dias R P, Yoo C S, Kim M, et al. Insulator-metal transition of highly compressed carbon disulfide[J]. *Physical Review B*, 2011, 84(14): 144104.
- [139] Kalosakas G, Aubry S, Tsironis G P. Possibility of observation of polaron normal modes at the far-infrared spectrum of acetanilide and related organics[J]. *Physics Letters A*, 1998, 247(6): 413-416.
- [140] Kick M, Scheurer C, Oberhofer H. Polaron-Assisted Charge Transport in Li-Ion Battery Anode Materials[J]. *ACS Applied Energy Materials*, 2021, 4(8): 8583-8591.
- [141] Peng C W, Liao W B, Chen T Y, et al. Efficient spin-orbit torque generation in semiconducting WTe₂ with hopping transport[J]. *ACS Applied Materials & Interfaces*, 2021, 13(13): 15950-15957.
- [142] Fetherolf, Jonathan H., Denis Gole z, and Timothy C. Berkelbach. "A unification of the Holstein polaron and dynamic disorder pictures of charge transport in organic crystals." *Physical Review X* 10.2 (2020): 021062.
- [143] Elmaslmane A R, Watkins M B, McKenna K P. First-principles modeling of polaron formation in TiO₂ polymorphs[J]. *Journal of chemical theory and computation*, 2018, 14(7): 3740-3751.
- [144] Chuang H J, Tan X, Ghimire N J, et al. High mobility WSe₂ p-and n-type field-effect transistors contacted by highly doped graphene for low-resistance contacts[J]. *Nano letters*, 2014, 14(6): 3594-3601.
- [145] Araki, Gako, et al. "Polaronlike vibrational bands of molecular crystals with one-dimensional hydrogen-bond chains: N-methylacetamide." *Physical Review B* 43.15 (1991): 12662.
- [146] Chang, Chun-Min, AH Castro Neto, and A. R. Bishop. "Long-range charge transfer in periodic DNA through polaron diffusion." *Chemical physics* 303.1-2 (2004): 189-196.

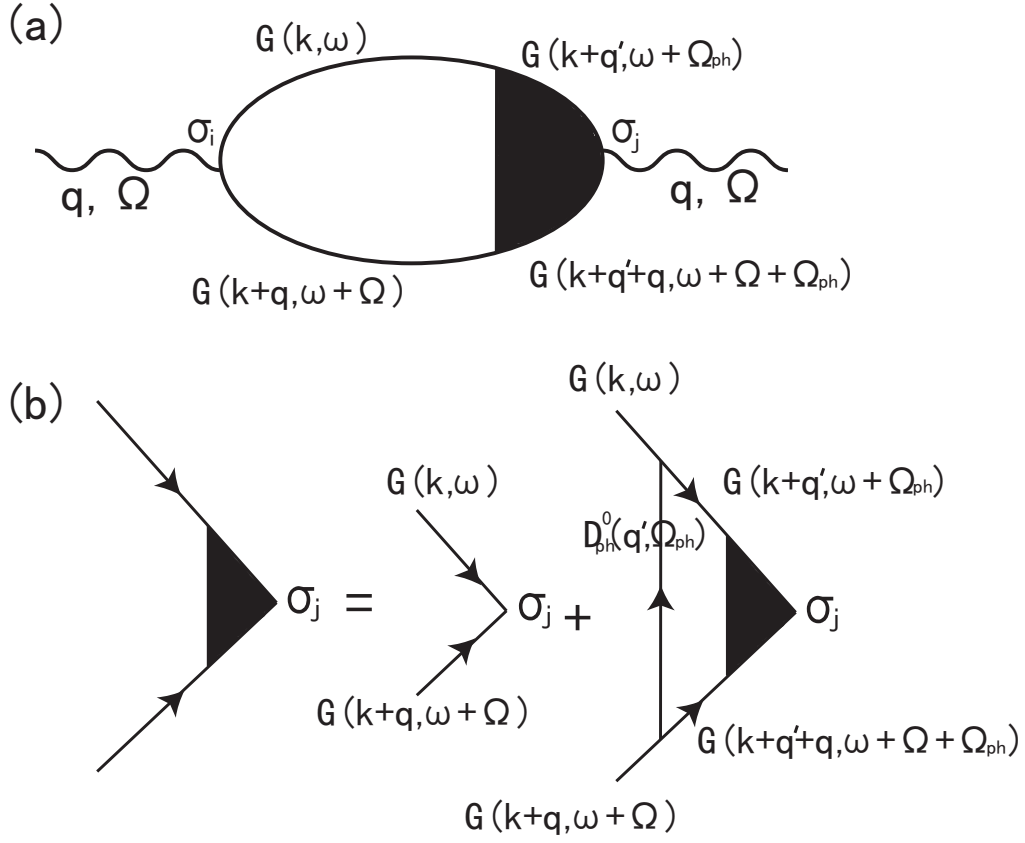


Figure 2: Real part (left) and imaginary part (right) of the pair propagator at non-chiral case as a function of the impurity momentum p and majority momentum q . The rows from top to bottom correspond to the Bosonic frequency (impurity) $\omega = -1, 0, 1, 2$, respectively. The momentum cutoff Λ is setted as 1 and the chemical potential is zero. The vertical axis is in unit of $\frac{1}{2\pi}$.

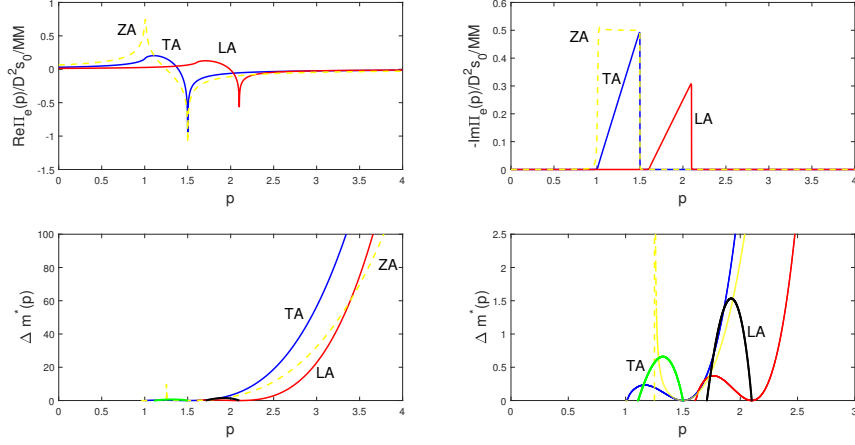


Figure 3: The upper panels show the real part and imaginary part of the self-energy induced by the electron-phonon coupling. For TA, LA, and ZA phonon modes, we apply the dispersions q' , $1.6q'$, and q'^2 respectively. The imaginary part of the self-energy here can also be regarded as the impurity scattering rate (inversed lifetime) according to the RPA. The third panel shows the induced effective masses by the electron-phonon coupling, and the green line and black line correspond to the induced effective masses calculated by the approximated expression for the TA and LA phonon, respectively. The chemical potential is setted as zero and the Debye radius is setted as $q_D = 1$. The impurity mass is also setted as 1. The last panel shows the enlarged view of the third panel.

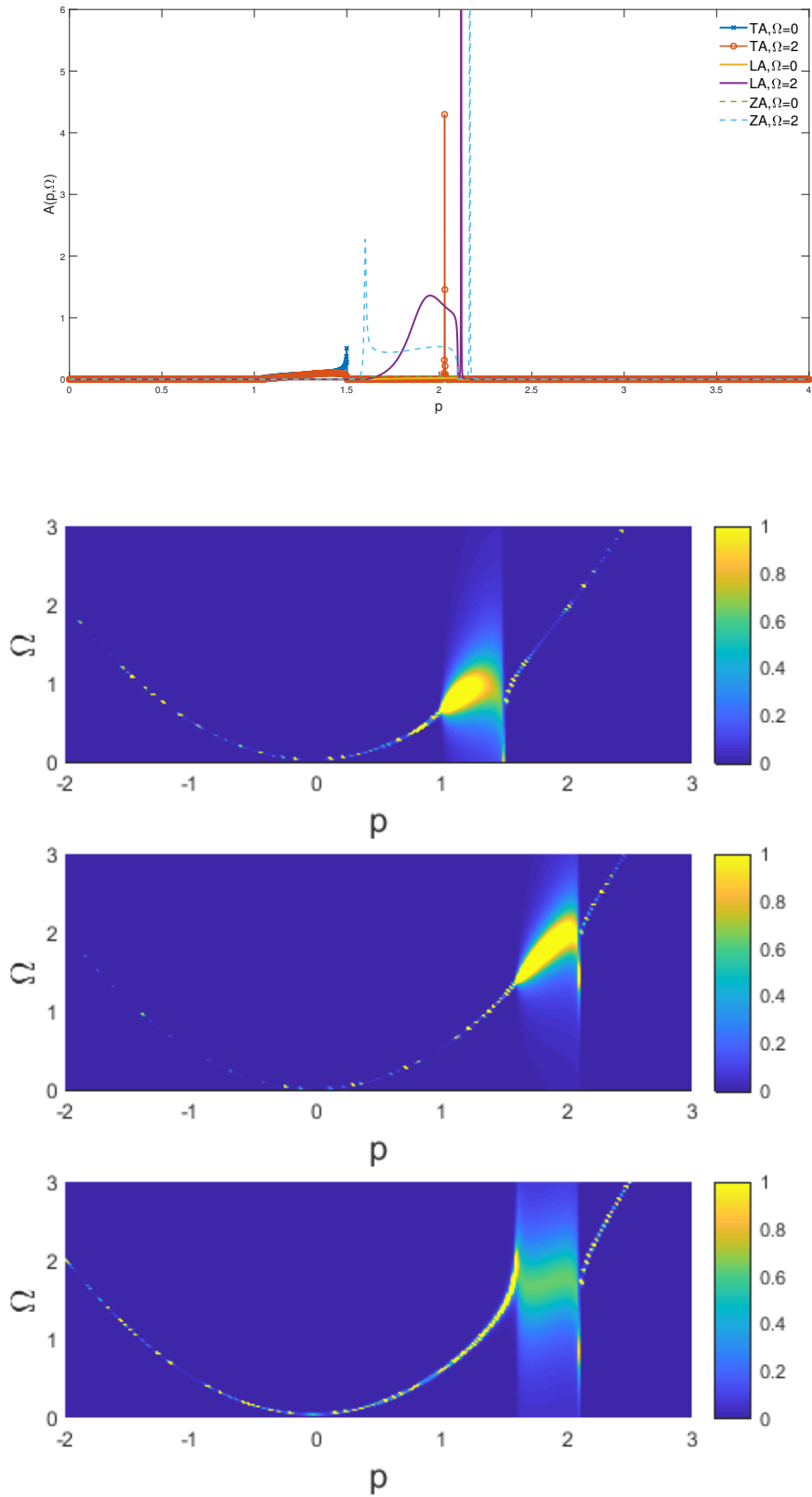


Figure 4: Polaron spectral function $A(p, \Omega)$ due to the electron-phonon coupling. The three intensity plots from top to the bottom correspond to the TA, LA, and ZA phonons.

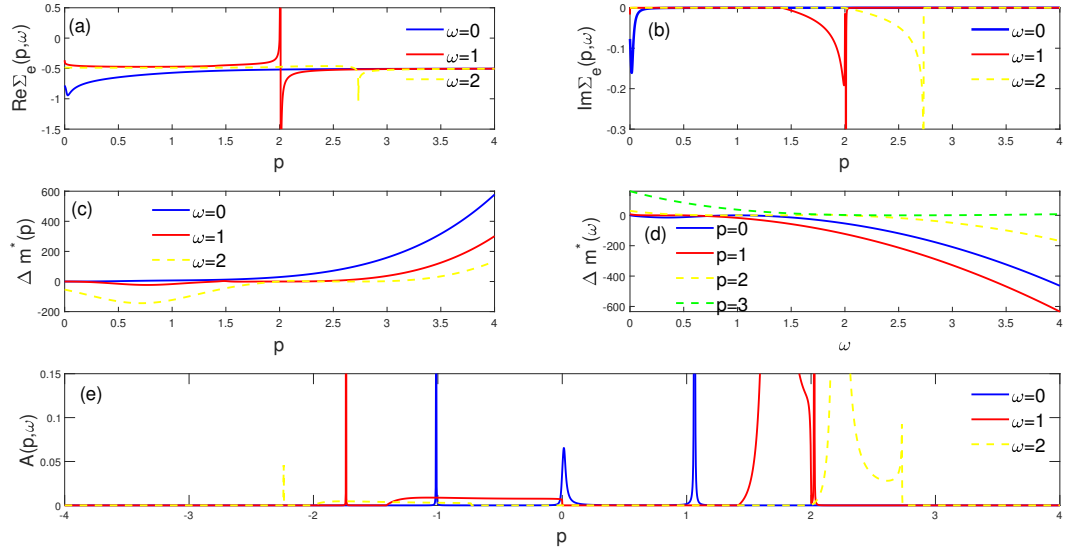


Figure 5: Real part (a) and imaginary part (b) of the self-energy induced by the interaction between impurity and the electron-hole pair (in coherence case). We set the chemical potential as zero, and bare coupling as $g_b = -0.5$. (c) and (d) shows the induced effective masses as a function of impurity momentum and frequency respectively. (e) shows the calculated spectral function as function of momentum. Here we only present the results for the bare coupling $g_b = -0.5$, but by changing the value of g_b , we obtain that the real part of self-energy (no matter how large the ω is) at large momentum will always equal to g_b , i.e., the attractive feature of the polaron enhanced by the increasing $|g_b|$, while the induced effective masses will decrease with the increase of $|g_b|$ ($g_b < 0$).

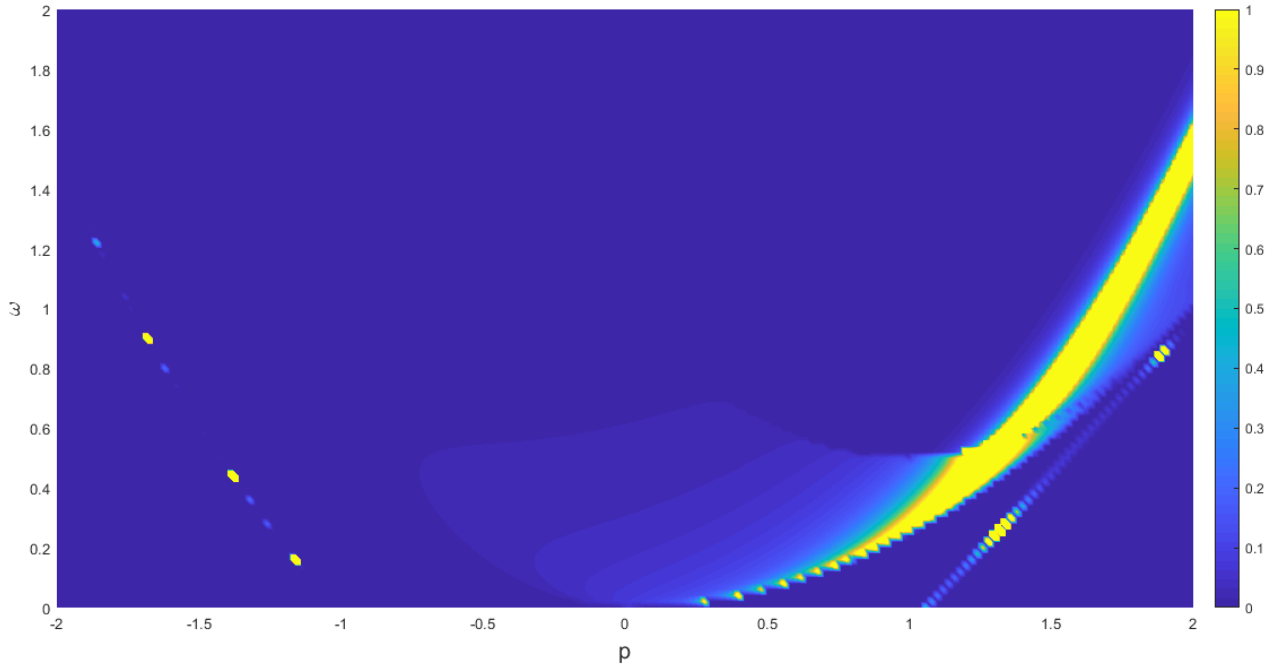


Figure 6: Intensity of the spectral function $A(p, \omega)$ due to the interaction between impurity and the electron-hole pair.

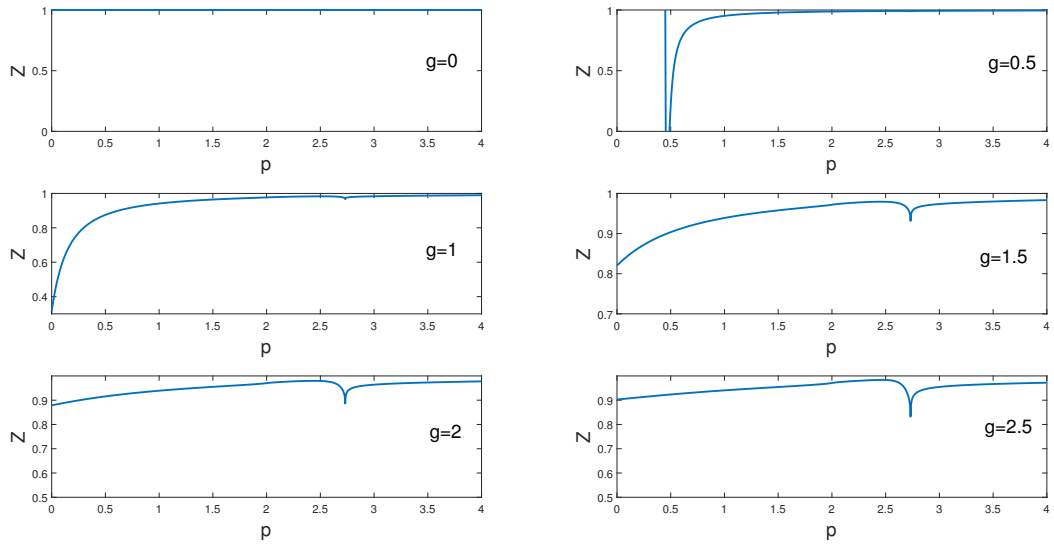


Figure 7: Quasiparticle residue.

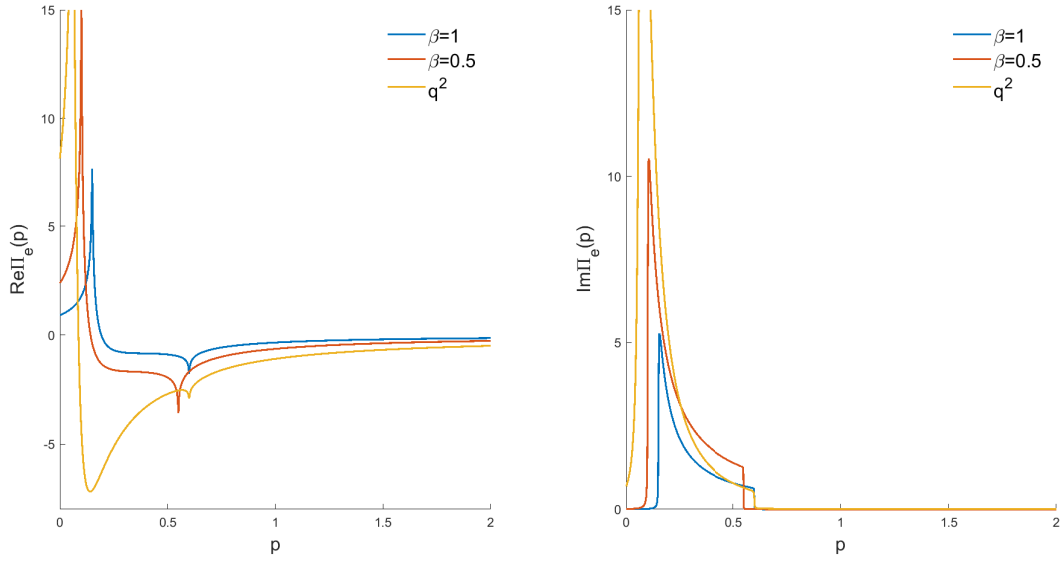


Figure 8: Electron self-energy induced by the electron-phonon interaction. The blue and red curves correspond to the linear phonon dispersion $\Omega_{ph}^0(q') = \beta q'$ (as found in the LA, TA branches in 2D hexagonal material) with $\beta = 1$ and $\beta = 0.5$, respectively. The yellow curve corresponds to $\Omega_{ph}^0(q') = q'^2$. The vertical axis is in unit of $(\frac{3\sqrt{3}t}{a\sqrt{4MN}})^2$. Here we apply the quadratic dispersion of the impurity, and we can see that the resulting impurity self-energy is momentum p -dependent. While for the Dirac dispersion, where the p -dependence vanishes due to the linear relation, and the resulting self-energy can be obtained as $-0.0793994839 + i(1.0702 \times 10^{-5})$, $-0.1561074601 + i(2.0684 \times 10^{-5})$, $-0.3732 + i(2.0348 \times 10^{-5})$ for the three cases of $\Omega_{ph}^0(q') = q'$, $\Omega_{ph}^0(q') = 0.5q'$, $\Omega_{ph}^0(q') = q'^2$, respectively. It is obvious that around a Dirac cone, the polaron formed by the coupling between electron and the lattice vibration mode is an attractive one and with much smaller imaginary part compared to the free electron.

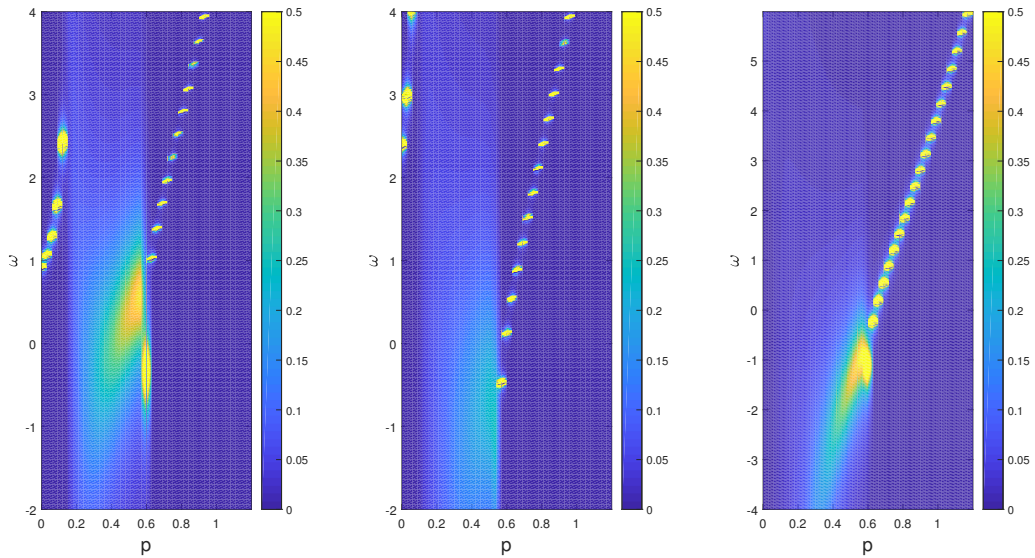


Figure 9: Spectral function according to the electron-phonon coupling induced self-energy. The left, middle, right panels are corresponding to the phonons with dispersion $\Omega_{ph}^0 = q'$, $0.5q'$, q'^2 , respectively. The bright regions are the polaronic modes induced by the electron-phonon coupling. In the region where the imaginary part of self-energy is large, the polaronic mode is been damped, resembling to the damping of other collective excitations in the single particle continuum regime.

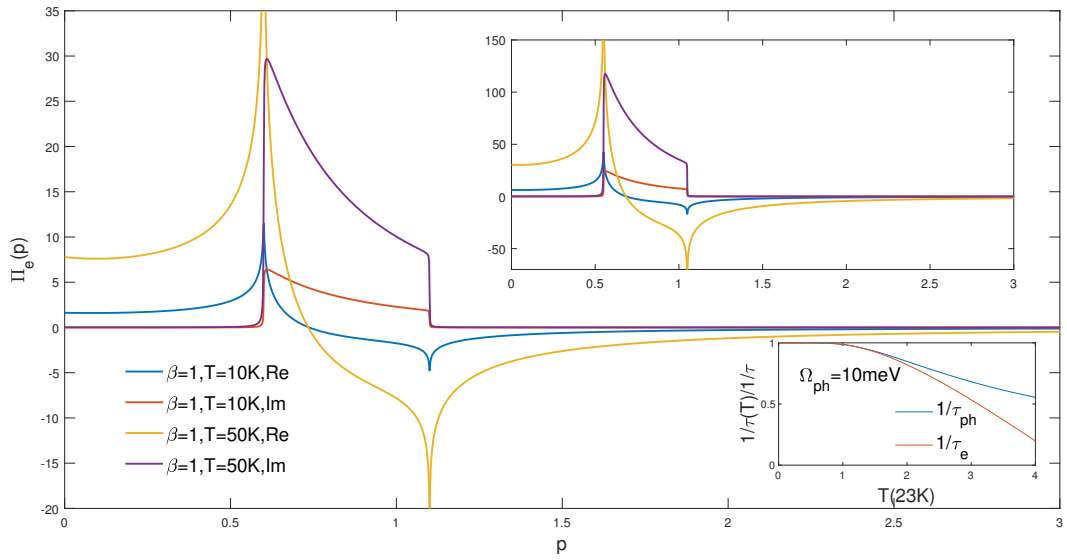


Figure 10: Electron self-energy induced by the electron-phonon interaction with $\beta = 1$ at finite temperature. The vertical axis is in unit of $(\frac{3\sqrt{3}t}{a\sqrt{4MN}})^2$. The upper inset shows the case with $\beta = 0.5$. Similar to the Fig.2, the peaks are higher in the case of small β , and such difference is more obvious at finite-temperature compared to the zero-temperature. The lower inset shows the temperature dependence of the electron linewidth ($1/\tau_e$) and the phonon linewidth ($1/\tau_{ph}$). Note that, for the calculation of the finite-temperature case, we use the approximation of the series expansion near zero phonon frequency $\Omega_{ph} \rightarrow 0$, thus the selection of q' is restricted within the small values.

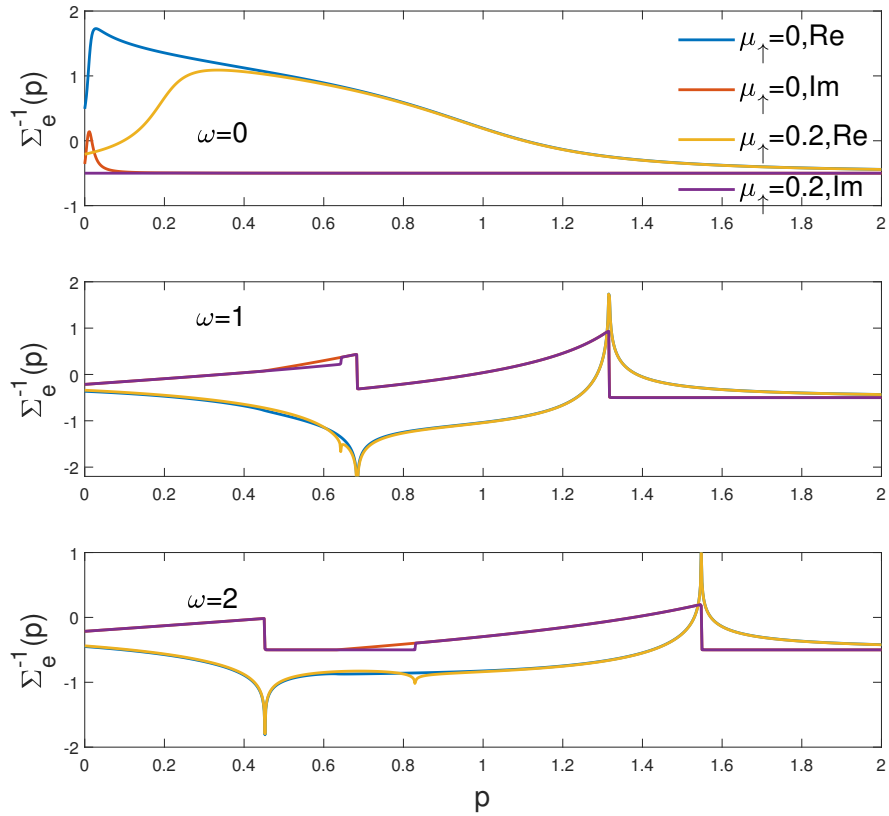


Figure 11: Electron self-energy induced by the interaction between impurity and the electron-hole pair. The curves for $\mu_\uparrow = 0$ and $\mu_\uparrow = 0.2$ are presented. Here $\mu_\uparrow \approx E_F$ in weak coupling BCS limit. We note that here the case of $\mu_\uparrow = 0$ corresponds to the vacuum limit[76] or the two-body limit, i.e., we only take one particle-hole excitation into account, which is applicable due to the destructive interference in a system with the superposition between states with different number of particle-hole pairs. We also set $q = 0$ here for the validity of one particle-hole part ansatz (see Ref.[95, 25]). The imaginary part of the self-energy also equal to the electron scattering rate $\hbar/2\pi\tau$.

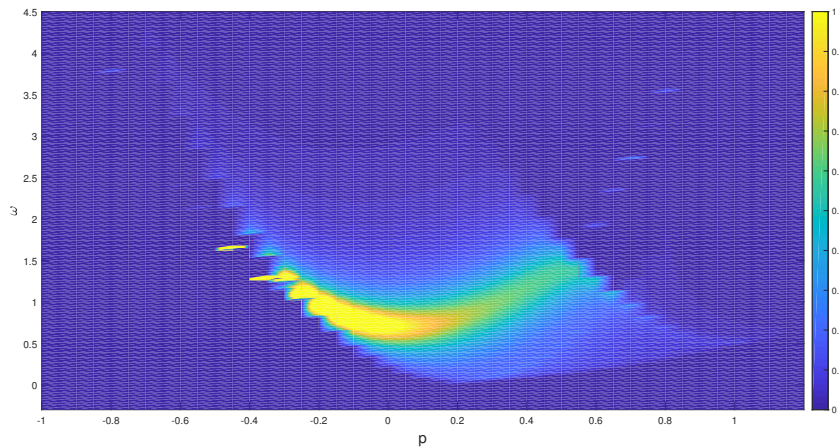


Figure 12: Spectral function of the fermi polaron self-energy.

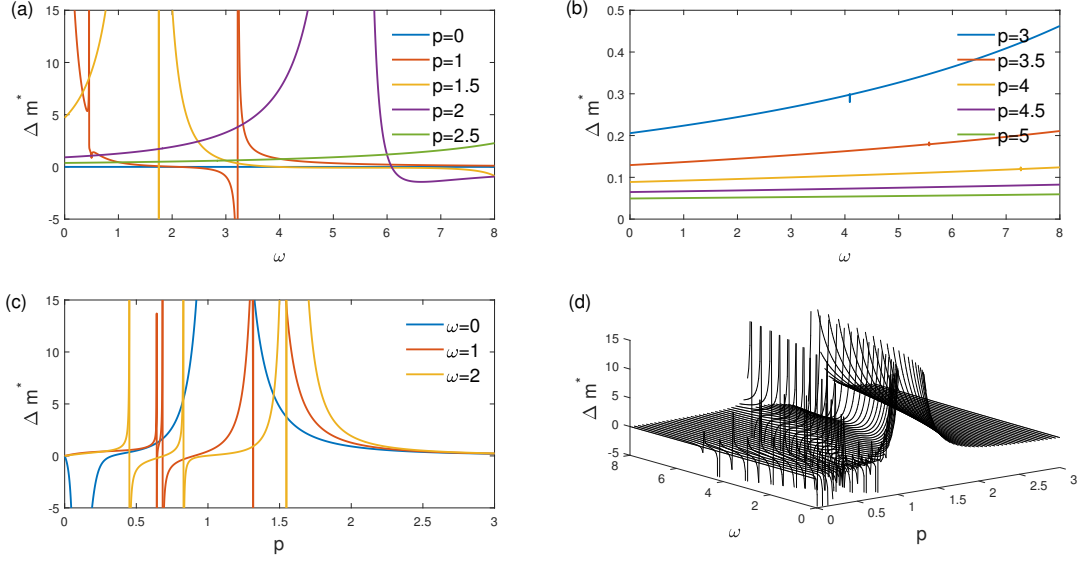


Figure 13: Effective mass induced by the interaction between impurity and the electron-hole pair in the strong coupling regime ($g^{-1}(\Lambda) \rightarrow 0$). Here we use the approximated expression of $\Delta m^*(p, \omega) = \frac{p}{\partial_p \Sigma_c(p, \omega)}$ [19, 1]. We set $\mu_\uparrow = k_F = 0.2$ here.

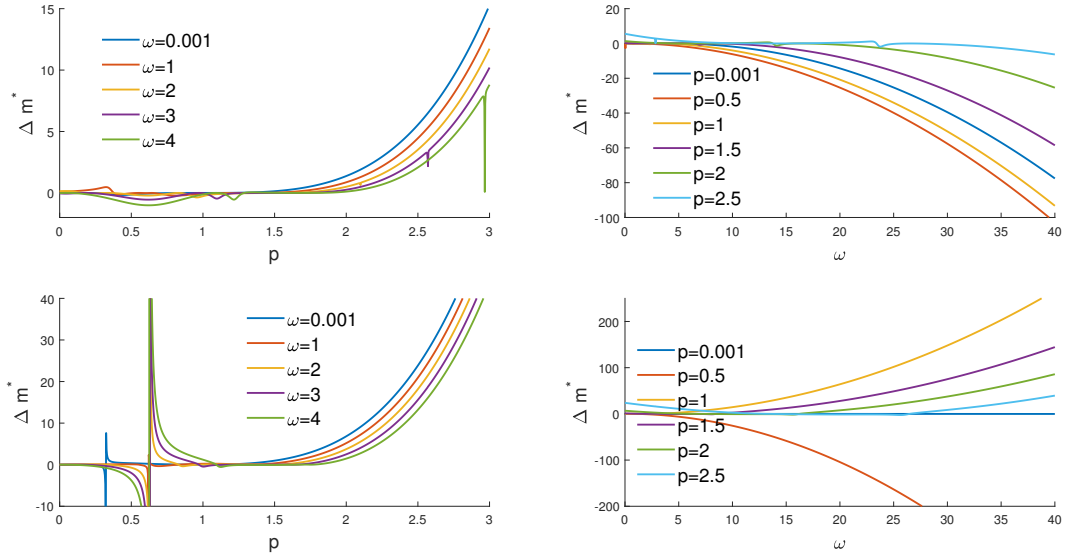


Figure 14: Effective mass induced by the interaction between impurity and the electron-hole pair with the bare coupling set as $(g^b)^{-1} = -0.5$. Exact expression (upper panels) approximated expression (lower panels) are used (see main text). We set $\mu_\uparrow = k_F = 0.2$ here.

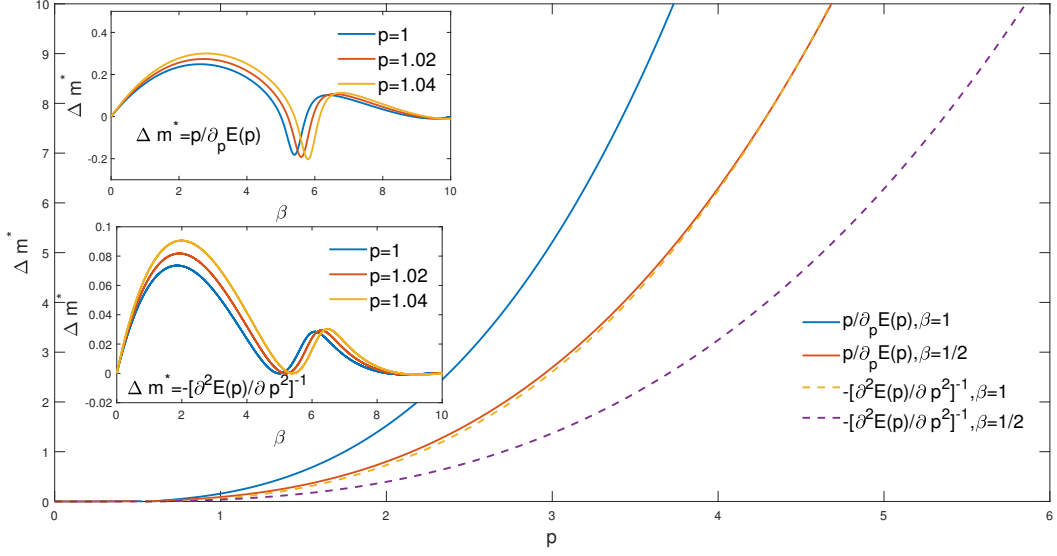


Figure 15: Effective mass induced by the electron-phonon coupling. We present both the approximation result of $m^* = \frac{p}{\partial_p E(p)}$ and the exact result $m^* = -[\frac{\partial^2 E(p)}{\partial p^2}]^{-1}$. We can clearly see that the expression of $m^* = \frac{p}{\partial_p E(p)}$ is applicable in the low-impurity-momentum region. We also present the effective mass as a function of slope rate of phonon spectrum base on these two expressions in the upper inset and lower inset, respectively. The difference is that the negative effective mass does not emerges in the lower inset (the exact result) which means that the electron-phonon coupling only increases the effective mass of the polaron. While for the upper inset for momentum $p \sim 1$, the negative effective mass emerges near the point $\beta = 5.5$.

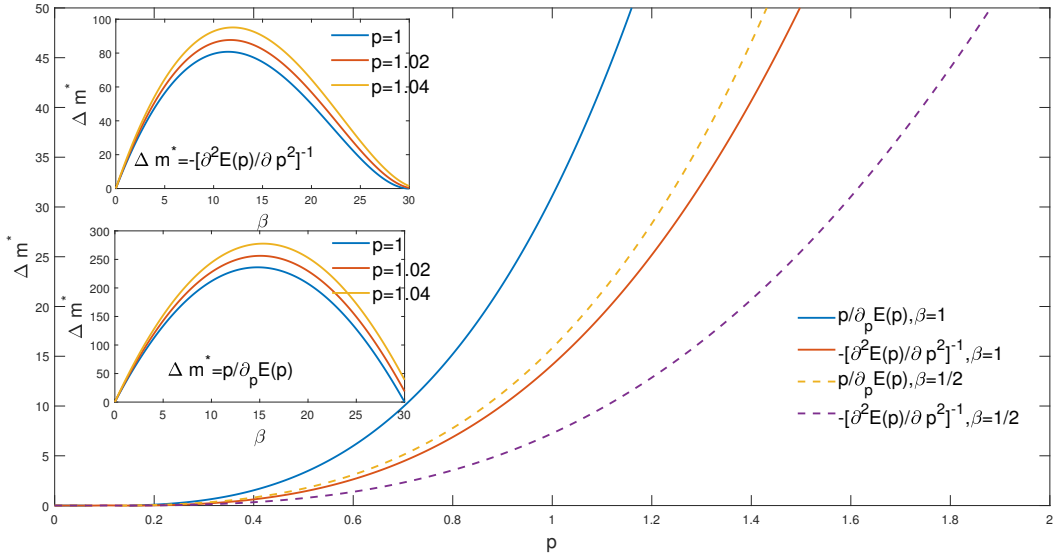


Figure 16: The same with Fig. 7 but for initial unperturbed impurity located near the Dirac cone. Here we set $\alpha \approx 30\beta$ (for LA) according to the first-principle calculations[24, 81].

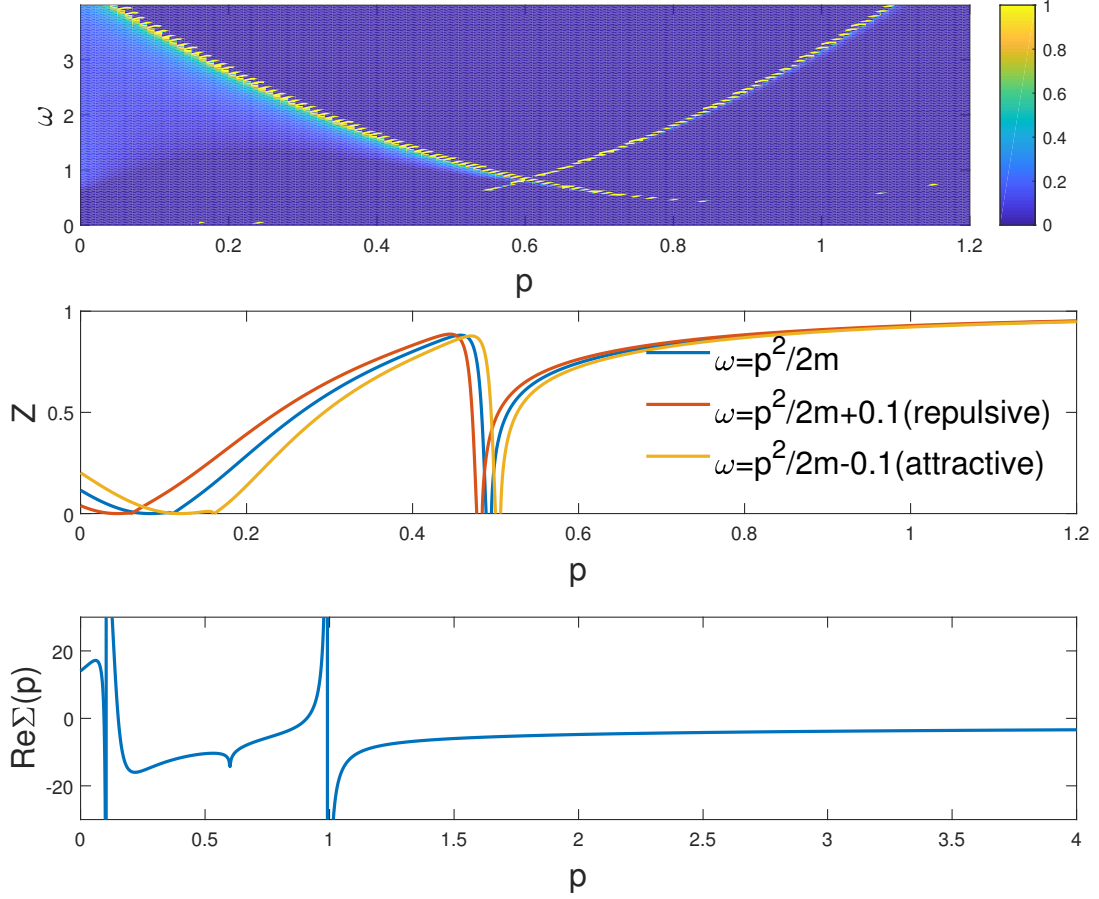


Figure 17: (upper panel) Two-dimensional map of the quasiparticle residue Z of the composite polaron. (middle panel) the approximated result of residue Z . (lower panel) the self-energy of the composite polaron. Note that here the residue in middle panel, which has two minimal singular points in $p = 0.1$ and $p = 0.5$, is not the exact result since the choosed impurity frequency ω is not exactly the pole of impurity Green's function. Through the lower panel, we can see that the imaginary part of self-energy induced instabilities are mainly located on the $p = 0.1$ and $p = 1$. Thus we can reasonably think that the two minimal singular points of exact residue should also located on the $p = 0.1$ and $p = 1$, rather than the $p = 0.1$ and $p = 0.5$.